

---

# Flightpath Synthesis and HUD Scaling for V/STOL Terminal Area Operations

---

Vernon K. Merrick and James A. Jeske, Ames Research Center, Moffett Field, California

April 1995



National Aeronautics and  
Space Administration

**Ames Research Center**  
Moffett Field, California 94035-1000



## SYMBOLS

It should be noted that although many of the symbols used in this report are defined similarly to those in references 1 and 2 there are instances where the definitions differ.

The symbols are divided into the following four categories:

1. Input variables (either from sensors or precomputed and stored).
2. Constant inputs (set by the pilot or frozen at flightpath select).
3. Derived variables used in the description of the flightpath and guidance laws.
4. Derived constants used in the description of the flightpath and guidance laws.

To create a degree of order, the following rules have been adopted in the assignment of mathematical symbols to the various quantities.

- All variables are designated by lower case symbols (Roman or Greek).
- With the exception of the acceleration due to gravity,  $g$ , all constants are designated by upper case symbols (Roman or Greek).
- A hat over a quantity (e.g.,  $\hat{x}$ ) denotes that it has been normalized by the true radius of the circle (acquiring or approach) with which it is associated.
- A numerical subscript associated with either a variable or a constant denotes its value in one of the nine coordinate frames of reference identified below.

### Coordinate frames of reference

#### Frames used in flightpath synthesis (fig. 2)

**Frame 1** The  $x$  axis points north, the  $y$  axis points east, and the origin is located at the landing pad datum.

**Frame 2** Fixed in the landing pad with the origin located at the landing pad datum.

**Frame 3** The  $x$  axis points along the aircraft's velocity vector, the  $y$  axis is clockwise to the  $x$  axis, and the origin is located at the aircraft's c.g.

#### Frames used to calculate the lateral guidance parameters (fig. 2)

**Frame 4** The  $x$  axis points along the initial straight segment, in the direction of flight; the  $y$  axis points in the direction of the concave side of the first blending curve; and the origin is located at the start of the first blending curve.

**Frame 5** The  $x$  axis points along the second straight segment, in the direction of flight; the  $y$  axis points in the direction of the convex side of the acquiring circle; and the origin is located at the center of the acquiring circle.

**Frame 6** The  $x$  axis points along the second straight segment, counter to the direction of flight; the  $y$  axis points in the direction of the concave side of the second blending curve; and the origin is located at the end of the second blending curve.

**Frame 7** The  $x$  axis points along the second straight segment, in the direction of flight; the  $y$  axis points in the direction of the concave side of the third blending curve; and the origin is located at the start of the third blending curve.

**Frame 8** The  $x$  axis points along the fourth and final straight segment, in the direction of flight; the  $y$  axis points in the direction of the convex side of the approach circle; and the origin is located at the center of the approach circle.

**Frame 9** The  $x$  axis points along the fourth and final straight segment, counter to the direction of flight; the  $y$  axis points in the direction of the concave side of the fourth blending curve; and the origin is located at the end of the fourth blending curve.

### (1) Input Variables

$h$	aircraft altitude, ft
$v_t$	aircraft groundspeed, ft/sec
$x_2, y_2$	aircraft coordinates in coordinate frame 2, ft
$\phi$	aircraft roll angle, deg
$\theta$	aircraft pitch angle, deg
$\psi$	aircraft heading, deg
$\psi_v$	heading of the aircraft's velocity vector, deg

### (2) Input Constants

$D_c$	nominal length of the final flightpath segment, ft
$D_i$	length of the initial straight flightpath segment (seg. 1), ft
$\hat{D}_i$	$D_i$ normalized by the nominal radius of the acquiring circle
$D_{SJ\beta}$	length of the final constant altitude segment, ft
$g$	acceleration due to gravity, ft/sec <sup>2</sup>
$H$	hover altitude, ft
$I_p$	pilot selection of the approach circle direction
$K_\epsilon$	HUD lateral scaling constant
$R_{a(min)}$	minimum nominal radius of the acquiring flightpath circle, ft
$R_{l(min)}$	minimum nominal radius of the approach flightpath circle, ft
$R_{(max)}$	maximum nominal radius of either the acquiring or the approach circle, ft
$R_{v_1}$	radius of segment $J_1J_2$ , ft
$R_{v_2}$	radius of segment $J_3J_4$ , ft
$S_{x_1}, S_{y_1}$	touchdown or station-keeping point in coordinate frame 1, ft
$X_{max}, X_{min}$	maximum and minimum $x$ (lateral) HUD coordinate, deg
$Y_{max}, Y_{min}$	maximum and minimum $y$ (vertical) HUD coordinate, deg
$\Delta D$	minimum desirable distance along the approach circle, ft

$\Gamma$	reference approach flightpath angle, deg
$\hat{\Upsilon}_p$	normalized maximum length of any blending curve
$\Psi$	landing pad heading, deg
$\Psi_f$	heading of the final flightpath segment, deg

### (3) Derived Variables

$a_{x_2}, a_{y_2}$	coordinates of point <i>A</i> in coordinate frame 2 prior to flightpath select, ft
$b_{x_2}, b_{y_2}$	coordinates of point <i>B</i> in coordinate frame 2 prior to flightpath select, ft
$c_{x_2}, c_{y_2}$	coordinates of point <i>C</i> in coordinate frame 2 prior to flightpath select, ft
$d$	range to the touchdown or station keeping point measured along the synthesized flightpath, ft
$d_a$	nominal range to point <i>A</i> , ft
$d_b$	nominal range to point <i>B</i> , ft
$d_d$	nominal range to point <i>D</i> , ft
$d_{a_0}$	nominal range to point <i>A</i> <sub>0</sub> , ft
$d_{x_2}, d_{y_2}$	coordinates of point <i>D</i> in coordinate frame 2 prior to flightpath select, ft
$h_g$	ghost aircraft altitude, ft
$i_a$	indicates clockwise ( $i_a = +1$ ) or counterclockwise ( $i_a = -1$ ) acquiring circle prior to flightpath select
$i_l$	indicates clockwise ( $i_l = +1$ ) or counterclockwise ( $i_l = -1$ ) approach circle prior to flightpath select
$l_a$	straight line distance from the aircraft to the center of the acquiring circle, ft
$l_{ac}$	straight line distance from the aircraft to the point at the start of the final straight segment (seg. 9), ft
$l_{al}$	length of the line connecting the centers of the acquiring and approach circles, ft
$l_{db}$	nominal length of the straight segment tangential to both the acquiring and approach circles, ft
$l_l$	straight line distance from the aircraft to the center of the approach circle, ft
$r_a$	nominal radius of the acquiring circle prior to flightpath select, ft
$r_{ax_2}, r_{ay_2}$	coordinates of the center of the acquiring circle in coordinate frame 2 prior to flightpath select, ft
$r_{ax_3}, r_{ay_3}$	coordinates of the center of the acquiring circle in coordinate frame 3 prior to flightpath select, ft
$r_l$	nominal radius of the approach circle prior to flightpath select, ft
$r_{lx_2}, r_{ly_2}$	coordinates of the center of the approach circle in coordinate frame 2 prior to flightpath select, ft
$r_{lx_3}, r_{ly_3}$	coordinates of the center of the approach circle in coordinate frame 3 prior to flightpath select, ft
$\hat{s}(\hat{x}, \hat{\Xi})$	normalized distance along the blending curve from the origin
$\hat{x}_4, \hat{y}_4$	normalized coordinates of the aircraft in coordinate frame 4
$x_5, y_5$	coordinates of the aircraft in coordinate frame 5, ft
$\hat{x}_6, \hat{y}_6$	normalized coordinates of the aircraft in coordinate frame 6

$\hat{x}_7, \hat{y}_7$	normalized coordinates of the aircraft in coordinate frame 7
$x_8, y_8$	coordinates of the aircraft in coordinate frame 8, ft
$\hat{x}_9, \hat{y}_9$	normalized coordinates of the aircraft in coordinate frame 9
$x_f, y_f$	unscaled coordinates of the flightpath symbol in the HUD coordinate frame, deg
$x_f^s, y_f^s$	scaled coordinates of the flightpath symbol in the HUD coordinate frame, deg
$x_g, y_g$	unscaled coordinates of the ghost symbol in the HUD coordinate frame, deg
$x_{g1}, y_{g1}$	unscaled coordinates of the ghost symbol without lateral position error in the HUD coordinate frame, deg
$x_g^s, y_g^s$	unscaled coordinates of the ghost symbol in the HUD coordinate frame, deg
$\hat{x}_p, \hat{y}_p$	normalized coordinates of the foot of the perpendicular from the aircraft to the blending curve
$\alpha_i$	inertial angle of attack, deg
$\alpha_m$	angle between a line connecting the centers of the acquiring and approach circles and the common tangent to the two circles (seg. 5), deg
$\alpha_v$	angle between the aircraft's velocity vector and the tangent to the approach circle passing through the aircraft, deg
$\beta_i$	inertial angle of sideslip, deg
$\delta h$	altitude error from the reference flightpath, ft
$\delta x_{gy}, \delta x_{gh}$	distances of the ghost aircraft ahead of the real aircraft for lateral and vertical tracking, ft
$\delta y$	lateral distance of the aircraft from the reference flightpath track, ft
$\delta \psi_{al}$	angle between the line connecting the centers of the acquiring and approach circles and the $x_2$ axis, deg
$\delta \psi_i$	angle between the tangent to the approach circle passing through the aircraft and the $x_2$ axis, deg
$\delta \psi_l$	angle between a line connecting the aircraft and the center of the approach circle ( $A_0L_c$ in fig. 1) and the $x_2$ axis, deg
$\delta \psi_s$	angle between the tangent common to the acquiring and approach circles and the $x_2$ axis, deg
$\delta \psi_v$	angle between the aircraft's velocity vector and the $x_2$ axis, deg
$\gamma_t$	reference flightpath angle at the aircraft's position, deg
$\lambda$	angle between a line from the aircraft to the center of the approach circle and a line tangential to the approach circle passing through aircraft, deg
$\nu$	angle subtended at the center of either the acquiring or approach circles by the parts of segments 3 or 7 yet to be traversed, deg
$\eta_g$	ghost aircraft elevation angle, deg
$\mu_g$	ghost aircraft azimuth angle, deg
$\mu_{g1}$	ghost aircraft azimuth angle without lateral tracking error, deg
$\nu_a$	nominal angle subtended at the center of the acquiring circle by the segment of the flightpath lying on the acquiring circle (seg. 3), deg
$\nu_l$	nominal angle subtended at the center of the approach circle by the segment of the flightpath lying on the approach circle (seg. 7), deg
$\nu'_l$	angle subtended at the center of the approach circle by the perpendiculars

to the final straight segment and the tangent to the approach circle passing through the aircraft, deg

$\rho$	radius of curvature of the reference flightpath track, ft
$\phi_g$	ghost aircraft roll angle, deg
$\psi_i$	heading of a tangent from the approach circle passing through the aircraft prior to the addition of the acquiring circle, deg
$\psi_s$	heading of the tangent common to the acquiring and approach circles, deg
$\psi_t$	heading of the tangent to the reference flightpath track at the aircraft's position, deg

#### (4) Derived Constants

$B_{x_2}, B_{y_2}$	coordinates of point $B$ in coordinate frame 2 after flightpath select, ft
$C_{x_2}, C_{y_2}$	coordinates of point $C$ in coordinate frame 2 after flightpath select, ft
$D_a$	range at point $A$ after flightpath select, ft
$D_{a_0}$	range at point $A_0$ after flightpath select, ft
$D_{a_1}$	range at point $A_1$ after flightpath select, ft
$D_{b_1}$	range at point $B_1$ after flightpath select, ft
$D_{b_2}$	range at point $B_2$ after flightpath select, ft
$D_{c_1}$	range at point $C_1$ after flightpath select, ft
$D_{c_2}$	range at point $C_2$ after flightpath select, ft
$D_{x_2}, D_{y_2}$	coordinates of point $D$ in coordinate frame 2 after flightpath select, ft
$D_{J_1}$	range at point $J_1$ (fig. 4), ft
$D_{J_2}$	range at point $J_2$ (fig. 4), ft
$D_{J_3}$	range at point $J_3$ (fig. 4), ft
$D_{J_4}$	range at point $J_4$ (fig. 4), ft
$D_{J_\alpha}$	range at point $J_\alpha$ (fig. 4), ft
$D_{J_\beta}$	range at point $J_\beta$ (fig. 4), ft
$E_a$	angle subtended by the blending curve at the center of the acquiring circle, deg
$E_l$	angle subtended by the blending curve at the center of the approach circle, deg
$\hat{F}_a$	nondimensional quantity used in evaluation of $\hat{X}_a$
$\hat{F}_l$	nondimensional quantity used in evaluation of $\hat{X}_l$
$I_a$	indicates clockwise ( $I_a = +1$ ) or counterclockwise ( $I_a = -1$ ) acquiring circle after flightpath select
$I_l$	indicates clockwise ( $I_l = +1$ ) or counterclockwise ( $I_l = -1$ ) approach circle after flightpath select
$H_{J_1}$	altitude at point $J_1$ (fig. 4), ft
$H_{J_2}$	altitude at point $J_2$ (fig. 4), ft
$H_{J_3}$	altitude at point $J_3$ (fig. 4), ft
$H_{J_4}$	altitude at point $J_4$ (fig. 4), ft
$H_{ri}$	altitude at flightpath select, ft
$H_\alpha$	altitude at point $J_\alpha$ (fig. 4), ft
$H_\beta$	altitude at point $J_\beta$ (fig. 4), ft

$R_a$	nominal radius of the acquiring circle after flightpath select, ft
$\bar{R}_a$	true radius of the acquiring flightpath circle after flightpath select, ft
$R_{ax_2}, R_{ay_2}$	coordinates of the center of the acquiring circle in coordinate frame 2, ft
$R_{ax_3}, R_{ay_3}$	coordinates of the center of the acquiring circle in coordinate frame 3, ft
$R_l$	nominal radius of the approach circle after flightpath select, ft
$\bar{R}_l$	true radius of the approach flightpath circle after flightpath select, ft
$R_{lx_2}, R_{ly_2}$	coordinates of the center of the approach circle in coordinate frame 2, ft
$R_{lx_3}, R_{ly_3}$	coordinates of the center of the approach circle in coordinate frame 3, ft
$\Delta\Psi_f$	angle between the final flightpath segment and the $x_2$ axis, deg
$\Delta\Psi_l$	angle between a line from the aircraft to the center of the reference flightpath circle and the $x_2$ axis, deg
$\Delta\Psi_i$	angle between the initial flightpath segment and the $x_2$ axis after flightpath select, deg
$\Lambda$	angle between a line from the aircraft to the center of the reference approach circle and the $x_2$ axis, deg
$N_a$	angle subtended at the center of the nominal acquiring circle by the complete arc of the acquiring circular segment, deg
$N_l$	angle subtended at the center of the nominal approach circle by the complete arc of the approach circular segment, deg
$\bar{N}_a$	angle subtended at the center of the true acquiring circle by the complete arc of the acquiring circular segment, deg
$\bar{N}_l$	angle subtended at the center of the true approach circle by the complete arc of the approach circular segment, deg
$\hat{\Upsilon}_a$	normalized blend parameter for the acquiring circle
$\hat{\Upsilon}_l$	normalized blend parameter for the approach circle
$\hat{\Upsilon}_{p(max)}$	maximum value of $\hat{\Upsilon}_p$
$\hat{X}_a$	nondimensional total length of the blending curve at the acquiring circle
$\hat{\bar{X}}_a$	nondimensional ordinate length of the portion of the blending curve lying within the arc of the nominal acquiring circle
$\hat{X}_l$	nondimensional total length of the blending curve to the approach circle
$\hat{\bar{X}}_l$	nondimensional ordinate length of the portion of the blending curve lying within the arc of the nominal approach circle
$\Psi_i$	heading of the initial straight flightpath segment, deg
$\Psi_v$	value of $\psi_v$ after flightpath select, deg
$\Psi_{vi}$	angle between the velocity vector and the initial flightpath segment at flightpath select, deg

### Acronyms

HUD	Head Up Display
IMC	Instrument Meteorological Conditions
VMC	Visual Meteorological Conditions
VMS	Vertical Motion Simulator
V/STOL	Vertical/Short Takeoff and Landing
VSRA	V/STOL Systems Research Aircraft



# FLIGHTPATH SYNTHESIS AND HUD SCALING FOR V/STOL TERMINAL AREA OPERATIONS

Vernon K. Merrick and James A. Jeske  
Ames Research Center

## SUMMARY

A two circle horizontal flightpath synthesis algorithm for Vertical/Short Takeoff and Landing (V/STOL) terminal area operations is presented. This algorithm provides a flightpath that is tangential to the aircraft's velocity vector at the instant of flightpath select and has continuous curvature. The algorithm corrects deficiencies noted in tests conducted with the V/STOL Systems Research Aircraft (VSRA) using a single circle algorithm described in NASA TM 104027. In addition, a more general vertical flightpath synthesis algorithm is presented, aimed primarily at minimizing the rapid increase of pilot workload during the final phase of decelerating transition just prior to acquiring the station-keeping point. Finally, a new technique for lateral scaling of a V/STOL Head Up Display (HUD) is presented, aimed at minimizing the inevitable anomalies that such scaling produces.

All the above named items have been tested in flight with the VSRA, and all have produced improvements.

## INTRODUCTION

In reference 1, a horizontal flightpath synthesis algorithm is presented for a particular class of flightpaths suitable for final approach to a Vertical/Short Takeoff and Landing (V/STOL) landing pad. This class, shown in figure 34 of reference 1, is defined by a straight segment starting at the aircraft and tangential to an approach circle of predefined radius, followed by a segment of the approach circle, and finally by a straight segment of predefined heading and length that is also tangential to the approach circle and ends at the hover station-keeping point adjacent to the landing pad. The algorithm selects one of the two possible approach circles depending on the location of the aircraft and according to the rules depicted in figure 34 of reference 1. Manned simulation in the Ames Research Center's Vertical Motion Simulator, on which the flightpath synthesis algorithm was evaluated, pointed to the need for two modifications (ref. 2) that were subsequently incorporated and flown in the V/STOL Systems Research Aircraft (VSRA) (ref. 3). One of these modifications was the addition of blending curves at the two points where the straight and circular segments meet in order to remove the curvature discontinuities. The other modification was the addition of an "acquiring curve" preceding the first straight flightpath segment, giving the pilot explicit guidance in aligning the aircraft's velocity vector with the first straight segment, and thereby avoiding guidance errors at the instant of flightpath select. The first mentioned modification was satisfactory. The second modification, which guided the pilot to perform an S turn, was satisfactory only if the final track change was less than about 15 deg. When the track change exceeded about 15 deg, the need to bank

the aircraft through a substantial angle in one direction followed by an immediate equal sized bank in the other direction is a high workload task at a point in the approach where such a task would not be performed by a pilot in an unguided approach.

The purpose of this report is to present an algorithm that provides a flightpath that is closer to one that would be performed by a pilot in an unguided approach. In essence the new algorithm replaces the acquiring curve with an "acquiring circle," hence the term "two circle algorithm." It follows that the S turn of the previous algorithm is replaced, in the new algorithm, by a single turn. In the same spirit, the vertical flightpath has been generalized to generate an approach path similar to that which Harrier pilots normally use. This flightpath differs from that given in reference 2 by the addition of a constant altitude final segment. The main advantage of this type of vertical flightpath is that it provides a time separation between the various control actions needed at the end of transition. Without the final constant altitude segment the pilot must continuously control errors in lateral position, altitude, speed, and distance to go. The addition of the constant altitude segment allows the pilot to establish the final altitude first and then concentrate on the lateral and longitudinal tasks. This approach is particularly effective in reducing pilot workload if the aircraft has a vertical speed command control system, since, once the final altitude is attained, the control system will maintain it without further pilot intervention.

The report starts with a description of the horizontal flightpath geometry in very general terms, followed by a list of the data needed for its generation. The equations and logic used in the synthesis procedure are given in two sections. The first section deals with the continuous synthesis prior to the flightpath selection by the pilot. The second section deals with additional calculations after flightpath select. A third section gives the lateral guidance equations. There then follows a description of the vertical flightpath geometry, along with sections, like those for the horizontal flightpath, dealing with the required data, the synthesis procedure, and the guidance equations.

It was pointed out in reference 2 that a satisfactory solution to the problem of Head Up Display (HUD) lateral scaling and limiting was not available and that any technique would result in anomalies of one kind or another. A recently devised technique, which shows promise of being satisfactory in that the attendant anomalies do not appear to be objectionable, is given in the last section of the report to show the direction of current thought on this subject.

## HORIZONTAL FLIGHTPATH SYNTHESIS

The flightpath (fig. 1) is constructed in the following way. Starting from any aircraft position,  $A_0$ , an initial straight segment,  $A_0A$ , is defined to be of preselected length oriented along the horizontal projection of the aircraft's velocity vector. A final straight segment,  $CS$ , is predefined to be of preselected length and approach track heading, ending at the station-keeping point  $S$ . Acquiring and approach circles are then defined that meet certain requirements. Principal requirements in locating the centers of these circles are that the

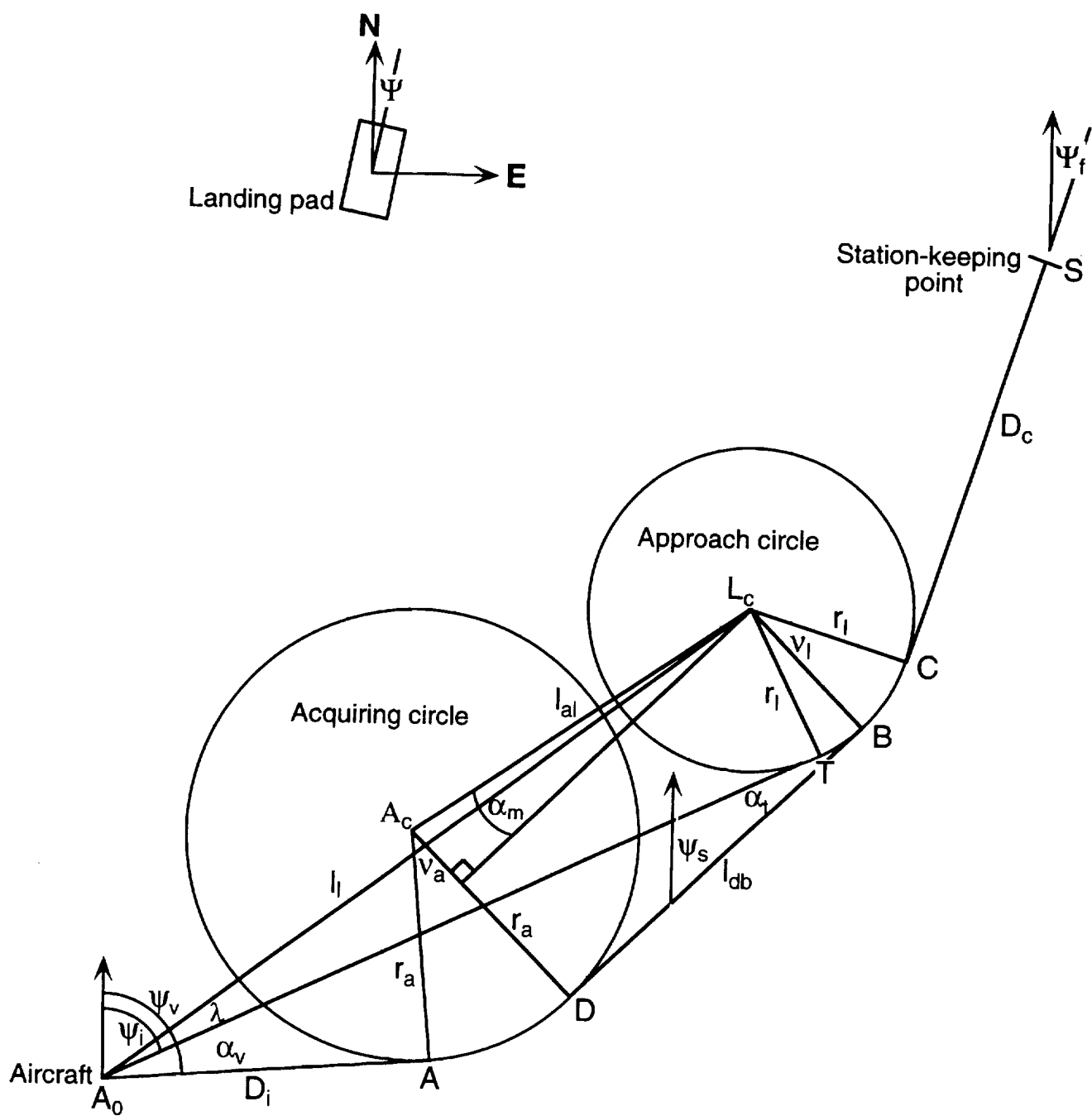


Figure 1. Geometry of the nominal flightpath.

initial straight segment be tangential to the acquiring circle and the final straight approach segment be tangential to the approach circle. The nominal flightpath is completed by the straight segment DB that is a common tangent to both circles. As with the previous synthesis (refs. 1 and 2), there are two possible approach circles corresponding to clockwise and counterclockwise approaches. Rather than have the algorithm select the approach circle to be used, as previously, the new algorithm requires the pilot to make the selection. However, the pilot also has the option of requesting the flightpath of minimum length, in which case the synthesis is performed for both approach circles and the one with minimum range is presented to the pilot. There are also two possible alternatives for the acquiring circle. The rule adopted here is that the circle selected is that whose center is located so that the aircraft is always directed to turn towards the tangent  $A_0T$  to the approach circle passing through the aircraft (fig. 1). Immediately after the flightpath has been selected, it is modified slightly to include cubic blending curves at the four points A, D, B, and C where the three tangents meet the two circles.

### Required Data

It is assumed that the on-board navigation sensors provide sufficient information and that there is sufficient processing capability to permit on-board continuous synthesis of a reference flightpath that is a member of the proposed class of flightpaths. When the synthesized flightpath is acceptable to the pilot he selects it by "freezing" the synthesizing process.

The set of constant parameters identified below must be provided to the synthesizing system so that it can construct an appropriate flightpath within the proposed class of flightpaths.

$D_c$	nominal length of the final flightpath segment $D_c > R_{l(min)} \Upsilon_p$
$D_i$	length of the initial straight flightpath segment $D_i > R_{a(min)} \Upsilon_p$
$I_p$	controls the pilot selection of the approach circle
$R_{a(min)}$	minimum nominal radius of the acquiring circle
$R_{l(min)}$	minimum nominal radius of the approach circle
$R_{(max)}$	maximum nominal radius of either the acquiring or approach circle
$S_{x_1}, S_{y_1}$	touchdown, or station-keeping point in coordinate frame 1 (see Symbols)
$\Delta D$	minimum distance flown along either the acquiring or approach circle $\Delta D < 2\hat{\Upsilon}_p(\text{minimum of } R_{a(min)} \text{ and } R_{l(min)})$
$\hat{\Upsilon}_p$	normalized value of the parameter defining the length of the blending curve ( $\hat{\Upsilon}_p \leq \sqrt{2/27}$ , ref. 2)
$\Psi$	landing pad heading ( $0 \leq \Psi < 360^\circ$ )
$\Psi_f$	heading of the final flightpath segment ( $0 \leq \Psi_f < 360^\circ$ )

These parameters are generally constant and have default values suitable for normal operational use, but, for research purposes, they may be changed, by the pilot, prior to the time the reference flightpath is selected. After the reference flightpath has been selected,

no further changes in these parameters can be made. In addition to these parameters, the navigation system must continuously provide the coordinates  $(x_1, y_1)$  of the aircraft in the north-east reference frame (frame 1) and the heading of the velocity vector,  $\psi_v$ .

### Calculations Before Flightpath Select

The coordinate frames of reference used to describe the flightpath algorithms are shown in figure 2.

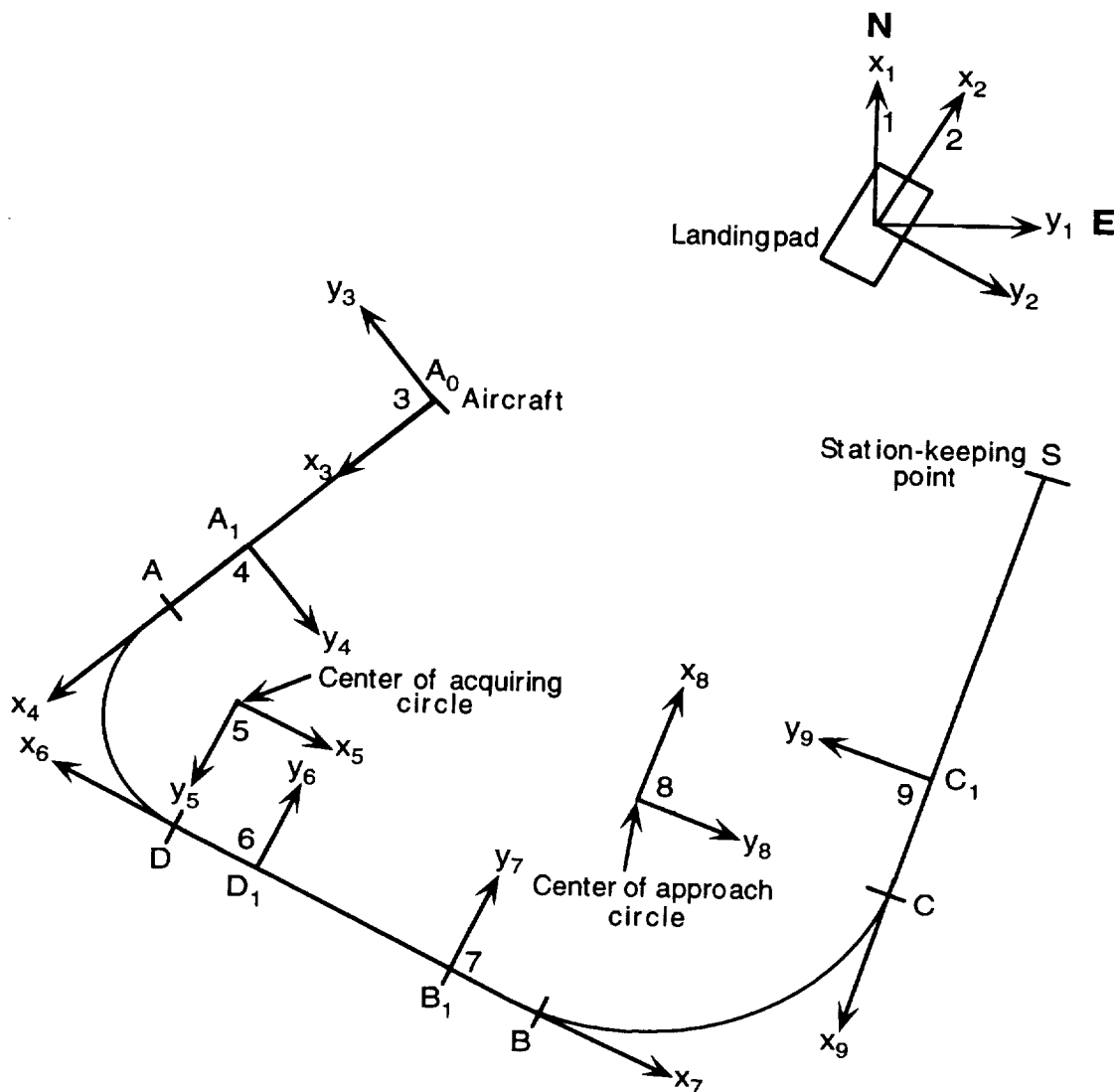


Figure 2. Coordinate frames of reference.

It is first required to convert the north-east coordinates (frame 1) of both the station-keeping point  $S$ ,  $(S_{x_1}, S_{y_1})$ , and the aircraft,  $(x_1, y_1)$ , to the landing pad coordinate system, (frame 2). The transformation equations are

$$S_{x_2} = S_{x_1} \cos \Psi + S_{y_1} \sin \Psi \quad (1)$$

$$S_{y_2} = S_{y_1} \cos \Psi - S_{x_1} \sin \Psi \quad (2)$$

and

$$x_2 = x_1 \cos \Psi + y_1 \sin \Psi \quad (3)$$

$$y_2 = y_1 \cos \Psi - x_1 \sin \Psi \quad (4)$$

where  $\Psi$  is the heading of the landing pad.

From the prescribed data, the heading of the final flightpath segment relative to the  $x$  axis of the landing pad,  $\Delta\Psi_f$ , is given by the equation

$$\Delta\Psi_f = \Psi_f - \Psi \quad 0 \leq \Delta\Psi_f < 360^\circ \quad (5)$$

and the coordinates of the point C (fig. 2) in frame 2,  $(C_{x_2}, C_{y_2})$ , are given by the equations

$$C_{x_2} = S_{x_2} - D_c \cos \Delta\Psi_f \quad (6)$$

$$C_{y_2} = S_{y_2} - D_c \sin \Delta\Psi_f \quad (7)$$

To avoid directing the pilot to make abrupt turns (caused by commanding inappropriately large bank angles for short periods of time when the track angle changes at the acquiring or approach circles are small), the radii of the two circles are set to ensure that the distance flown along either circle is not less than a specified value,  $\Delta D$ . However, as implied in the "Required Data" this rule only holds provided the radii are less than a specified value,  $R_{(max)}$ . This specified upper limit is made sufficiently large (say, 30,000 ft) that the bank angles required are too small to be objectionable.

To determine the appropriate acquiring and approach circle radii,  $r_a$  and  $r_l$ , they are first set equal to the minimum values,  $R_{a(min)}$  and  $R_{l(min)}$ , as specified in the "Required Data."

The coordinates  $(r_{lx_2}, r_{ly_2})$  of the center of the approach circle, in coordinate frame 2, are given by the equations

$$r_{lx_2} = C_{x_2} - i_l r_l \sin \Delta\Psi_f \quad (8)$$

$$r_{ly_2} = C_{y_2} + i_l r_l \cos \Delta\Psi_f \quad (9)$$

where  $i_l$  indicates which of the two approach circles is to be used ( $i_l = +1$  for clockwise and  $i_l = -1$  for counterclockwise). The value of  $i_l$  is identical to that of  $I_p$  when the value of  $I_p$ , set by the pilot, is either  $+1$  or  $-1$ . If the pilot sets  $I_p$  to zero, then flightpaths are synthesized for both  $i_l = +1$  and  $i_l = -1$  and the one that minimizes the range to point  $S$  (station-keeping point) is selected.

Given the approach circle to be flown, it is now required to determine which of the two possible acquiring circles is to be flown. This determination depends on the sign of the angle  $\alpha_v$  between the aircraft's velocity vector and the line  $A_0T$  (fig. 1). To determine  $\alpha_v$ , it is first required to calculate the length  $l_l$  of the line  $A_0L_c$  from the aircraft to the center of the approach circle, the angle  $\delta\psi_l$  between the line  $A_0L_c$  and the  $x$  axis of the landing pad, and the angle  $\lambda$  between the lines  $A_0L_c$  and  $A_0T$  (fig. 1). These three quantities are calculated from the equations

$$l_l = \sqrt{(x_2 - r_{lx_2})^2 + (y_2 - r_{ly_2})^2} \quad (10)$$

$$\delta\psi_l = \frac{180}{\pi} \tan^{-1} \left( \frac{r_{ly_2} - y_2}{r_{lx_2} - x_2} \right) \quad 0 \leq \delta\psi_l < 360^\circ \quad (11)$$

$$\lambda = \frac{180}{\pi} \sin^{-1} \left( \frac{r_l}{l_l} \right) \quad (12)$$

It follows from equation 12 that a path does not exist if  $r_l/l_l > 1$  and this information must be presented to the pilot. In this event the alternate approach direction will most likely yield a flightpath. In the unlikely event that neither approach direction yields a flightpath then the aircraft must be flown to a more appropriate position and track heading relative to the landing pad. In practice it is desirable to present the continuously synthesized flightpath on a display so that the pilot can instantly review the situation.

The angle between the line  $A_0T$  and the  $x_2$  axis of the landing pad,  $\delta\psi_i$ , may now be calculated from the equation

$$\delta\psi_i = \delta\psi_l - i_l \lambda \quad 0 \leq \delta\psi_i < 360^\circ \quad (13)$$

from which the heading  $\psi_i$  of the line  $A_0T$  is given by the equation

$$\psi_i = \Psi + \delta\psi_i \quad 0 \leq \psi_i < 360^\circ \quad (14)$$

The required angle  $\alpha_v$  is then given by the expression

$$\alpha_v = \psi_v - \psi_i \quad 0 \leq \alpha_v < 360 \quad (15)$$

The acquiring circle selected is characterized by  $i_a$ , where  $i_a = +1$  or  $-1$  denotes clockwise or counterclockwise, respectively. If  $\alpha_v \geq 180^\circ$ , then  $i_a = +1$  and if  $\alpha_v < 180^\circ$ , then  $i_a = -1$ .

It is now required to calculate the center of the acquiring circle in frame 2. The coordinates  $(r_{ax_3}, r_{ay_3})$  of the center of the acquiring circle in frame 3 can be obtained, by inspection, from figure 1 as

$$r_{ax_3} = D_i \quad (16)$$

$$r_{ay_3} = i_a r_a \quad (17)$$

To obtain the coordinates of the acquiring circle in frame 2, it is required to know the angle  $\delta\psi_v$  between the aircraft's velocity vector and the  $x$  axis of the landing pad.

$$\delta\psi_v = \psi_v - \Psi \quad 0 \leq \psi_i < 360^\circ \quad (18)$$

The coordinates  $(r_{ax_2}, r_{ay_2})$  of the center of the acquiring circle in frame 2 are obtained by rotation through the angle  $\delta\psi_v$  and translation from point  $A_0$  to the landing pad datum.

$$r_{ax_2} = x_2 + r_{ax_3} \cos \delta\psi_v - r_{ay_3} \sin \delta\psi_v \quad (19)$$

$$r_{ay_2} = y_2 + r_{ay_3} \cos \delta\psi_v + r_{ax_3} \sin \delta\psi_v \quad (20)$$

It is now required to calculate the angle  $\alpha_m$  between the line  $A_c L_c$  connecting the centers of the acquiring and approach circles and the tangent DB (fig. 1), common to the two circles. To calculate this angle it is first necessary to determine the angle  $\delta\psi_{al}$  between the line  $A_c L_c$  and the  $x$  axis of the landing pad ( $x_2$  axis), along with the length  $l_{al}$  of the line  $A_c L_c$ . The angle  $\delta\psi_{al}$  is given by the expression

$$\delta\psi_{al} = \frac{180}{\pi} \tan^{-1} \left( \frac{r_{ly_2} - r_{ay_2}}{r_{lx_2} - r_{ax_2}} \right) \quad 0 \leq \delta\psi_{al} < 360 \quad (21)$$

and the distance  $l_{al}$  by the expression

$$l_{al} = \sqrt{(r_{lx_2} - r_{ax_2})^2 + (r_{ly_2} - r_{ay_2})^2} \quad (22)$$

The angle  $\alpha_m$  then follows from the equation

$$\alpha_m = \frac{180}{\pi} \sin^{-1} \left( \frac{r_a - i_a i_l r_l}{l_{al}} \right) \quad 0 \leq \alpha_m < 360 \quad (23)$$



which takes into consideration the specific acquiring and approach circles through the quantities  $i_a$  and  $i_l$ .

It follows from equation 23 that if  $|r_a - i_a i_l r_l|/l_{al} > 1$  then a flightpath is not available within the constraints of the synthesizing algorithm for the approach circle requested (i.e., value of  $i_l$ ), and, again, this information must be presented to the pilot.

The angle  $\delta\psi_s$  between the tangent DB, common to the two circles, and the  $x_2$  axis may now be calculated from the expression

$$\delta\psi_s = \delta\psi_{al} + i_a \alpha_m \quad (24)$$

and the heading of this line by the expression

$$\psi_s = \delta\psi_s + \Psi \quad 0 \leq \psi_s < 360^\circ \quad (25)$$

The nominal angles,  $\nu_a$  and  $\nu_l$ , of the flightpath circular arcs subtended at the centers of the acquiring and approach circles may now be calculated from the equations

$$\nu_a = -i_a(\psi_v - \psi_s) \quad 0 \leq \nu_a < 360 \quad (26)$$

$$\nu_l = 180(1 + i_l) - i_l(\psi_s - \Psi_f) \quad \nu_l < 360 \quad (27)$$

In order to calculate the various nominal ranges at key points, the length  $l_{db}$  of the tangent DB, common the acquiring and approach circles, is required. This quantity is calculated from the equation

$$l_{db} = l_{al} \cos \alpha_m \quad (28)$$

At this point it is required to review, and possibly modify, the circle radii in accordance with the rule specified earlier. This procedure is most conveniently expressed in the following pseudocode.

IF  $\nu_a \neq 0$  THEN

$$r_a \leftarrow \Delta D / \nu_a \quad (29)$$

$$\text{IF } r_a < R_{a(min)} \quad r_a = R_{a(min)} \quad (30)$$

$$\text{IF } r_a > R_{a(max)} \quad r_a = R_{a(max)} \quad (31)$$

ELSE

$$r_a = R_{a(max)} \quad (32)$$

ENDIF

IF  $\nu_l \neq 0$  THEN

$$r_l \leftarrow \Delta D / \nu_l \quad (33)$$

$$\text{IF } r_l < R_{l(min)} \quad r_l = R_{l(min)} \quad (34)$$

$$\text{IF } r_l > R_{l(max)} \quad r_l = R_{l(max)} \quad (35)$$

IF  $r_l > R_{l(min)}$  THEN

$$r_{lx_2} = C_{x_2} - i_l r_l \sin \Delta \Psi_f$$

$$r_{ly_2} = C_{y_2} + i_l r_l \cos \Delta \Psi_f$$

ENDIF

ELSE

$$r_l = R_{l(max)} \quad (36)$$

ENDIF

If the value of either of the circle radii are changed then the calculations from equations 8–28 are repeated. Then the radii tests given in equations 29–36 are skipped and the remaining calculations performed.

The key nominal ranges (i.e., not allowing for the effect of the blending curves) at points  $B$ ,  $D$ ,  $A$ , and  $A_0$  can now be calculated sequentially from the following expressions:

$$d_b = D_c + r_l \nu_l \quad (37)$$

$$d_d = d_b + l_{db} \quad (38)$$

$$d_a = d_d + r_a \nu_a \quad (39)$$

$$d_{a_0} = d_a + D_i \quad (40)$$

Guidance calculations, after the flightpath has been selected by the pilot, require the coordinates of points  $A$ ,  $B$ , and  $D$  in frame 2. These coordinates may be obtained from the following expressions:

$$a_{x_2} = x_2 + D_i \cos \delta \psi_v \quad (41)$$

$$a_{y_2} = y_2 + D_i \sin \delta \psi_v \quad (42)$$

$$b_{x_2} = r_{lx_2} + i_l r_l \sin \delta \psi_s \quad (43)$$

$$b_{y_2} = r_{ly_2} - i_l r_l \cos \delta \psi_s \quad (44)$$

$$d_{x_2} = b_{x_2} - l_{db} \cos \delta \psi_s \quad (45)$$

$$d_{y_2} = b_{y_2} - l_{db} \sin \delta \psi_s \quad (46)$$

Note that the coordinates of point  $C$ ,  $(C_{x_2}, C_{y_2})$ , are given by equations 6 and 7 and depend only on data specified by the pilot.

The quantities  $i_a$ ,  $i_l$ ,  $\delta \psi_i$ ,  $\psi_i$ ,  $\delta \psi_v$ ,  $\psi_v$ ,  $\delta \psi_s$ ,  $\psi_s$ ,  $a_{x_2}$ ,  $a_{y_2}$ ,  $b_{x_2}$ ,  $b_{y_2}$ ,  $d_{x_2}$ ,  $d_{y_2}$ ,  $l_{db}$ ,  $r_l$ ,  $r_{lx_2}$ ,  $r_{ly_2}$ ,  $r_a$ ,  $r_{ax_2}$ ,  $r_{ay_2}$ ,  $\nu_a$ , and  $\nu_l$  are calculated continuously up to the instant that the pilot selects the reference flightpath. After the flightpath has been selected, these quantities remain constant at their values at the instant of flightpath selection and they are subsequently designated by the uppercase symbols  $I_a$ ,  $I_l$ ,  $\Delta \Psi_i$ ,  $\Psi_i$ ,  $\Delta \Psi_v$ ,  $\Psi_v$ ,  $\Delta \Psi_s$ ,  $\Psi_s$ ,  $A_{x_2}$ ,  $A_{y_2}$ ,  $B_{x_2}$ ,  $B_{y_2}$ ,  $D_{x_2}$ ,  $D_{y_2}$ ,  $L_{db}$ ,  $R_l$ ,  $R_{lx_2}$ ,  $R_{ly_2}$ ,  $R_a$ ,  $R_{ax_2}$ ,  $R_{ay_2}$ ,  $N_a$ , and  $N_l$ , respectively.

A program was written, for an Apple Macintosh computer, to give a graphical representation of the nominal horizontal flightpath given by equations 1-46. This program was written to permit rapid validation of the equations by allowing easy modification of the input quantities. To aid the reader in assessing the scope of flightpath variations implied by the equations, the program is included in this report on a standard 3.5 inch floppy disk. The operating instructions for the program are provided in the Appendix.

### Calculations After Flightpath Select

Immediately after selection of the nominal flightpath, it is required to add the blending curves (fig. 3). The analysis leading to the required equations is given in reference 2. The process first requires the assignment of suitable values to the blending curve constants  $\hat{\Upsilon}_a$  and  $\hat{\Upsilon}_l$ . It is important to recognize that the values assigned to  $\hat{\Upsilon}_a$  and  $\hat{\Upsilon}_l$  cannot be greater than those which cause the blending curves for entry and exit to meet in the middle of a circular segment (ref. 2), and that one or both of these values may be less than the specified value of  $\hat{\Upsilon}_p$ . The equations expressing these limitations in the calculations of  $\hat{\Upsilon}_a$  and  $\hat{\Upsilon}_l$  are given in the following pseudocode:

$$\text{IF } N_a \leq (360/\pi) \sin^{-1} \sqrt{(1/6)} \text{ THEN} \\ \hat{\Upsilon}_{p(max)} \Leftarrow \sin(N_a/2) - 2[\sin(N_a/2)]^3 \quad (47)$$

$$\text{IF } \hat{\Upsilon}_p > \hat{\Upsilon}_{p(max)} \quad \hat{\Upsilon}_a \Leftarrow \hat{\Upsilon}_{p(max)} \quad (48)$$

$$\text{ELSE} \\ \hat{\Upsilon}_a \Leftarrow \hat{\Upsilon}_p \quad (49)$$

ENDIF

$$\text{IF } N_l \leq (360/\pi) \sin^{-1} \sqrt{(1/6)} \text{ THEN} \\ \hat{\Upsilon}_{p(max)} \Leftarrow \sin(N_l/2) - 2[\sin(N_l/2)]^3 \quad (50)$$

$$\text{IF } \hat{\Upsilon}_p > \hat{\Upsilon}_{p(max)} \quad \hat{\Upsilon}_l \Leftarrow \hat{\Upsilon}_{p(max)} \quad (51)$$

$$\text{ELSE} \\ \hat{\Upsilon}_l \Leftarrow \hat{\Upsilon}_p \quad (52)$$

ENDIF

To obtain the other blending curve constants (ref. 2) for the acquiring circle, we first define a quantity  $\hat{F}_a$  as follows:

$$\hat{F}_a \stackrel{\text{def}}{=} \cos^{-1} \left( -\hat{\Upsilon}_a \sqrt{\frac{27}{2}} \right) \quad (53)$$

The normalized distance  $\hat{X}_a$  (fig. 3)—measured along the straight segment—over which the blending curve replaces part of the circular arc segment is then given by

$$\hat{X}_a = \sqrt{\frac{2}{3}} \cos \left( \frac{\hat{F}_a + 4\pi}{3} \right) \quad (54)$$

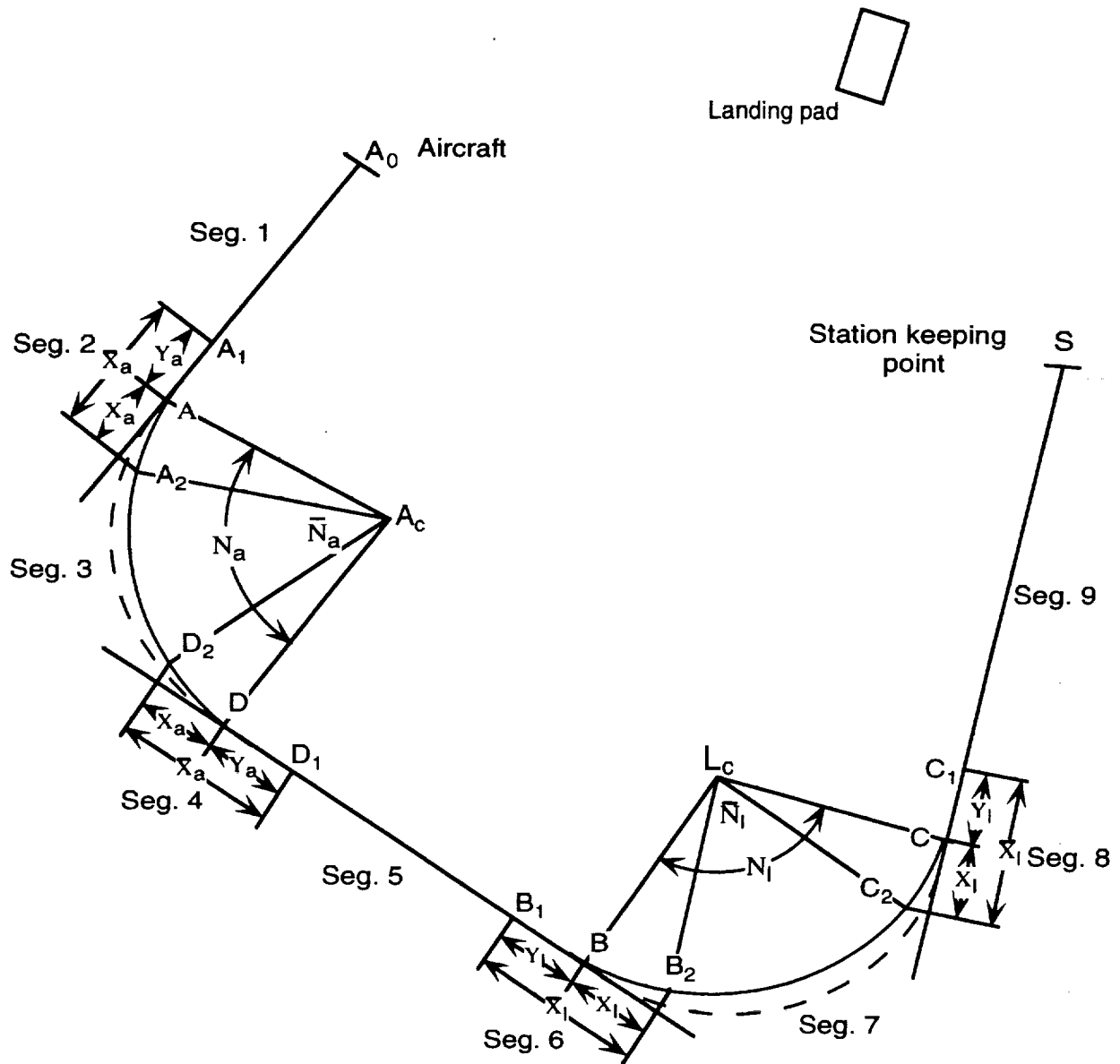


Figure 3. Geometry of the flightpath after pilot select.

and the normalized distance  $\hat{X}_a$  (fig. 3)—measured along the straight segment—over which the blending curve replaces part of the straight segment is then given by

$$\hat{X}_a = \hat{\bar{X}}_a + \hat{Y}_a \quad (55)$$

The defining constant of the cubic blending curves for the acquiring circle,  $\hat{\Xi}_a$ , is then calculated from the equation

$$\hat{\Xi}_a = \frac{\hat{X}_a}{3\hat{X}_a^2\sqrt{1-\hat{X}_a^2}} \quad (56)$$

If  $\hat{\Upsilon}_a = 0$ , then  $\hat{X}_a$  and  $\hat{X}_a$  are both zero and  $\hat{\Xi}_a$  from equation 56 is indeterminate. In order to recover the flightpath synthesis equations appropriate to the case where  $\hat{\Upsilon}_a = 0$ , it is necessary to define  $\hat{\Xi}_a$  to be zero.

The true radius,  $\bar{R}_a$ , of the acquiring circle is obtained from the nominal radius,  $R_a$ , using the equation

$$\bar{R}_a = \frac{R_a}{\hat{\Xi}_a\hat{X}_a^3 + \sqrt{1-\hat{X}_a^2}} \quad (57)$$

If the quantity  $E_a$  is defined by

$$E_a \stackrel{\text{def}}{=} \sin^{-1} \hat{X}_a \quad (58)$$

then the true flightpath circular segment lying on the acquiring circle subtends an angle  $\bar{N}_a$  given by

$$\bar{N}_a = N_a - 2E_a \quad (59)$$

The blending curve constants for the approach circle are given by the following set of equations similar to those given above for the acquiring circle

$$\hat{F}_l \stackrel{\text{def}}{=} \cos^{-1} \left( -\hat{\Upsilon}_l \sqrt{\frac{27}{2}} \right) \quad (60)$$

$$\hat{X}_l = \sqrt{\frac{2}{3}} \cos \left( \frac{\hat{F}_l + 4\pi}{3} \right) \quad (61)$$

$$\hat{X}_l = \hat{\hat{X}}_l + \hat{\Upsilon}_l \quad (62)$$

$$\hat{\Xi}_l = \frac{\hat{\hat{X}}_l}{3\hat{X}_l^2\sqrt{1-\hat{X}_l^2}} \quad (63)$$

$$\bar{R}_l = \frac{R_l}{\hat{\Xi}_l\hat{X}_l^3 + \sqrt{1-\hat{X}_l^2}} \quad (64)$$

$$E_l \stackrel{\text{def}}{=} \sin^{-1} \hat{X}_l \quad (65)$$

$$\bar{N}_l = N_l - 2E_l \quad (66)$$

Again, if  $\hat{Y}_l = 0$ , then it is necessary to define  $\hat{E}_l$  to be zero.

Equations 53-66 complete the calculation of the blending curve constants and it now remains to calculate the key ranges, measured along the true reference flightpath, at points  $C_1, C_2, B_1, B_2, D_1, D_2, A_1, A_2$ , and  $A_0$ . To obtain these ranges, it is necessary to calculate the lengths of the four principal segments of the blending curve corresponding to the normalized abscissa  $\hat{Y}_a, \hat{Y}_l, \hat{X}_a$ , and  $\hat{X}_l$ . These lengths can be obtained from the equation

$$\hat{s}(\hat{x}, \hat{E}) = \hat{x} + 0.9\hat{E}^2\hat{x}^5 - 1.125\hat{E}^4\hat{x}^9$$

where

$$\begin{array}{ll} \hat{x} & \text{normalized blending curve abscissa} \\ \hat{s}(\hat{x}, \hat{E}) & \text{normalized length of the blending curve} \end{array}$$

The key true ranges (i.e., allowing for the effect of the blending curves)  $D_{c_1}, D_{c_2}, D_{b_2}, D_{b_1}, D_{a_2}, D_{a_1}$ , and  $D_{a_0}$  are then calculated sequentially from the equations

$$D_{c_1} = D_c - \bar{R}_l \hat{Y}_l \quad (67)$$

$$D_{c_2} = D_{c_1} + \bar{R}_l \hat{s}(\hat{X}_l, \hat{E}_l) \quad (68)$$

$$D_{b_2} = D_{c_2} + \frac{\pi \bar{R}_l \bar{N}_l}{180} \quad (69)$$

$$D_{b_1} = D_{b_2} + D_{c_2} - D_{c_1} \quad (70)$$

$$D_{d_1} = D_{b_1} + L_{db} - \bar{R}_l \hat{Y}_l - \bar{R}_a \hat{Y}_a \quad (71)$$

$$D_{d_2} = D_{d_1} + \bar{R}_a \hat{s}(\hat{Y}_a, \hat{E}_a) \quad (72)$$

$$D_{a_2} = D_{d_2} + \frac{\pi \bar{R}_a \bar{N}_a}{180} \quad (73)$$

$$D_{a_1} = D_{a_2} + D_{d_2} - D_{d_1} \quad (74)$$

$$D_{a_0} = D_{a_1} + D_i - \bar{R}_a \hat{Y}_a \quad (75)$$

The quantities  $\bar{R}_a, \bar{R}_l, \hat{E}_a, \hat{E}_l, D_{a_0}, D_{a_1}, D_{a_2}, D_{b_1}, D_{b_2}, D_{c_1}, D_{c_2}, D_{d_1}$ , and  $D_{d_2}$  are calculated, once only, for subsequent use in the guidance equations.

It follows from equations 67 and 75 that there are restrictions on the pilot's specification of the nominal lengths of both the final and initial straight segments,  $D_c$  and  $D_i$ , since clearly (fig. 3) they must be large enough to make  $D_{c_1} > 0$  and  $D_{a_0} > D_{a_1}$ . The simplest way to express the needed restrictions is to relate them to the values of  $R_{a(min)}, R_{l(min)}$ , and  $\hat{Y}_p$  set by the pilot. If the values of  $D_c$  and  $D_i$  satisfy the inequalities  $D_c > R_{l(min)} \hat{Y}_p$

and  $D_i > R_{a(min)} \hat{\Upsilon}_p$  and if  $\Delta D < 2\hat{\Upsilon}_p$  (minimum of  $R_{a(min)}$  and  $R_{l(min)}$ ) then the desired distance relationships will be satisfied, although the inequalities do not necessarily identify the minimum possible values for  $D_c$  or  $D_i$ .

It also follows from equation 71 that a path will exist only if the exit blending curve for the acquiring circle and the entry blending curve for the approach circle do not overlap. Therefore, if  $D_{d_1} - D_{b_1} < 0$  (fig. 3) a suitable flightpath does not exist.

### Lateral Guidance

Lateral guidance is provided by the ghost-aircraft symbol, and the lateral-guidance law is provided by the geometrical relationship between the flightpath symbol and the ghost (fig. 16 of ref. 1). To calculate the azimuth angle of the ghost,  $\mu_g$ , requires knowledge of the range,  $d$ , the lateral offset of the aircraft from the reference-flightpath track,  $\delta y$ , and the heading of the reference flightpath,  $\psi_t$ . In addition, the ghost bank angle,  $\phi_g$ , given by

$$\phi_g = \frac{180}{\pi} \tan^{-1} \left( \frac{v_t^2}{\rho g} \right) \quad (76)$$

requires knowledge of the aircraft's true speed,  $v_t$ , and the reference flightpath curvature,  $1/\rho$ , at the aircraft's position (identified by its range,  $d$ ).

The quantities  $I_a, I_l, \Delta\Psi_i, \Psi_i, \Delta\Psi_v, \Psi_v, \bar{R}_a, \bar{R}_l, R_{ax_2}, R_{ay_2}, R_{lx_2}, R_{ly_2}, \bar{N}_a, \bar{N}_l, \hat{\Upsilon}_a, \hat{\Upsilon}_l, A_{x_2}, A_{y_2}, B_{x_2}, B_{y_2}, C_{x_2}, C_{y_2}, D_{x_2}, D_{y_2}, D_{a_0}, D_{a_1}, D_{a_2}, D_{b_1}, D_{b_2}, D_{c_1}, D_{c_2}, D_{d_1}$ , and  $D_{d_2}$  have been calculated by the flightpath synthesis algorithm and are constant thereafter.

The equations to determine the guidance quantities  $d, \delta y, \psi_t$ , and  $1/\rho$  depend on whether the segment is straight, a blending curve, or a circular arc. The derivations of these equations are self-evident for segments that are either straight or a circular arc. The more complicated equations for the blending curve are derived in reference 2. The independent quantities in these equations are the above-named flightpath constants and the aircraft's position coordinates,  $(x_2, y_2)$ , from equations 3 and 4. The set of equations for each of the nine segments of the complete flightpath (fig. 3) is given below.

For segments  $A_0A_1$  and  $A_1B_1$  (fig. 3), the normalized coordinates of the aircraft,  $(\hat{x}_4, \hat{y}_4)$ , in coordinate frame 4 (fig. 2), are given by

$$\hat{x}_4 = [(x_2 - A_{x_2}) \cos \Delta\Psi_v + (y_2 - A_{y_2}) \sin \Delta\Psi_v] / \bar{R}_a + \hat{\Upsilon}_a \quad (77)$$

$$\hat{y}_4 = I_a [(y_2 - A_{y_2}) \cos \Delta\Psi_v - (x_2 - A_{x_2}) \sin \Delta\Psi_v] / \bar{R}_a \quad (78)$$

Initial straight segment  $A_0A_1$  (seg. 1) defined by  $D_{a_0} \geq d > D_{a_1}$

$$d = D_{a_1} - \bar{R}_a \hat{x}_4 \quad (79)$$

$$\delta y = I_a \bar{R}_a \hat{y}_4 \quad (80)$$

$$\psi_t = \Psi_v \quad 0 \leq \psi_t < 360^\circ \quad (81)$$

$$\frac{1}{\rho} = 0 \quad (82)$$

Turn-entry blending curve to the acquiring circle  $A_1 A_2$  (seg. 2) defined by  $D_{a_1} \geq d > D_{a_2}$

$$\hat{x}_p = \hat{x}_4 \left[ 1 + \frac{3\hat{\Xi}_a \hat{x}_4 (\hat{y}_4 - \hat{\Xi}_a \hat{x}_4^3)}{1 - 3\hat{\Xi}_a \hat{x}_4 (2\hat{y}_4 - 5\hat{\Xi}_a \hat{x}_4^3)} \right] \quad (83)$$

$$\hat{y}_p = \hat{\Xi}_a \hat{x}_p^3 \quad (84)$$

$$d = D_{a_1} - \bar{R}_a \hat{s}(\hat{x}_p, \hat{\Xi}_a) \quad (85)$$

$$\delta y = \text{sign}(\hat{y}_4 - \hat{\Xi}_a \hat{x}_4^3) I_a \bar{R}_a \sqrt{(\hat{x}_4 - \hat{x}_p)^2 + (\hat{y}_4 - \hat{y}_p)^2} \quad (86)$$

$$\psi_t = \Psi_v + \frac{I_a 180}{\pi} \tan^{-1}(3\hat{\Xi}_a \hat{x}_p^2) \quad 0 \leq \psi_t < 360^\circ \quad (87)$$

$$\frac{1}{\rho} = \frac{I_a 6\hat{\Xi}_a \hat{x}_p}{\bar{R}_a (1 + 9\hat{\Xi}_a^2 \hat{x}_p^4)^{3/2}} \quad (88)$$

Circular segment on the acquiring circle  $A_2 D_2$  (seg. 3) defined by  $D_{a_2} \geq d > D_{d_2}$

$$x_5 = (x_2 - R_{ax_2}) \cos \Delta \Psi_s + (y_2 - R_{ay_2}) \sin \Delta \Psi_s \quad (89)$$

$$y_5 = I_a [(x_2 - R_{ax_2}) \sin \Delta \Psi_s - (y_2 - R_{ay_2}) \cos \Delta \Psi_s] \quad (90)$$

$$\nu = \frac{180}{\pi} \tan^{-1} \left( \frac{-x_5}{y_5} \right) \quad 0 \leq \nu < 360^\circ \quad (91)$$

$$d = D_{d_2} + \frac{\pi}{180} \bar{R}_a (\nu - E_a) \quad (92)$$

$$l_a = \sqrt{x_5^2 + y_5^2} \quad (93)$$

$$\delta y = I_a (\bar{R}_a - l_a) \quad (94)$$

$$\psi_t = \Psi_s - I_a \nu \quad 0 \leq \psi_t < 360^\circ \quad (95)$$

$$\frac{1}{\rho} = \frac{I_a}{\bar{R}_a} \quad (96)$$

where  $(x_5, y_5)$  are the coordinates of the aircraft in coordinate frame 5 (fig. 2).

Turn-exit curve from the acquiring circle  $D_2 D_1$  (seg. 4) defined by  $D_{d_2} \geq d > D_{d_1}$

$$\hat{x}_6 = -[(x_2 - D_{x_2}) \cos \Delta \Psi_s + (y_2 - D_{y_2}) \sin \Delta \Psi_s] / \bar{R}_a + \hat{\Upsilon}_a \quad (97)$$



$$\hat{y}_6 = I_a[(y_2 - D_{y_2}) \cos \Delta \Psi_s - (x_2 - D_{x_2}) \sin \Delta \Psi_s] / \bar{R}_a \quad (98)$$

$$\hat{x}_p = \hat{x}_6 \left[ 1 + \frac{3\hat{\Xi}_a \hat{x}_6 (\hat{y}_6 - \hat{\Xi}_a \hat{x}_6^3)}{1 - 3\hat{\Xi}_a \hat{x}_6 (2\hat{y}_6 - 5\hat{\Xi}_a \hat{x}_6^3)} \right] \quad (99)$$

$$\hat{y}_p = \hat{\Xi}_a \hat{x}_p^3 \quad (100)$$

$$d = D_{d_1} + \bar{R}_a \hat{s}(\hat{x}_p, \hat{\Xi}_a) \quad (101)$$

$$\delta y = \text{sign}(\hat{y}_6 - \hat{\Xi}_a \hat{x}_6^3) I_a \bar{R}_a \sqrt{(\hat{x}_6 - \hat{x}_p)^2 + (\hat{y}_6 - \hat{y}_p)^2} \quad (102)$$

$$\psi_t = \Psi_s - \frac{I_a 180}{\pi} \tan^{-1}(3\hat{\Xi}_a \hat{x}_p^2) \quad 0 \leq \psi_t < 360^\circ \quad (103)$$

$$\frac{1}{\rho} = \frac{I_a 6 \hat{\Xi}_a \hat{x}_p}{\bar{R}_a (1 + 9\hat{\Xi}_a^2 \hat{x}_p^4)^{3/2}} \quad (104)$$

For segments  $D_1 B_1$  and  $B_1 B_2$ , the normalized coordinates of the aircraft  $(\hat{x}_7, \hat{y}_7)$ , in coordinate frame 7 (fig. 2), are given by

$$\hat{x}_7 = [(x_2 - B_{x_2}) \cos \Delta \Psi_s + (y_2 - B_{y_2}) \sin \Delta \Psi_s] / \bar{R}_l + \hat{\Upsilon}_l \quad (105)$$

$$\hat{y}_7 = I_l [(y_2 - B_{y_2}) \cos \Delta \Psi_s - (x_2 - B_{x_2}) \sin \Delta \Psi_s] / \bar{R}_l \quad (106)$$

Second straight segment  $D_1 B_1$  (seg. 5) defined by  $D_{d_1} \geq d > D_{b_1}$

$$d = D_{b_1} - \bar{R}_l \hat{x}_7 \quad (107)$$

$$\delta y = I_l \bar{R}_l \hat{x}_7 \quad (108)$$

$$\psi_t = \Psi_s \quad 0 \leq \psi_t < 360^\circ \quad (109)$$

$$\frac{1}{\rho} = 0 \quad (110)$$

Turn-entry blend segment to the approach circle  $B_1 B_2$  (seg. 6) defined by  $D_{b_1} \geq d > D_{b_2}$

$$\hat{x}_p = \hat{x}_7 \left[ 1 + \frac{3\hat{\Xi}_l \hat{x}_7 (\hat{y}_7 - \hat{\Xi}_l \hat{x}_7^3)}{1 - 3\hat{\Xi}_l \hat{x}_7 (2\hat{y}_7 - 5\hat{\Xi}_l \hat{x}_7^3)} \right] \quad (111)$$

$$\hat{y}_p = \hat{\Xi}_l \hat{x}_p^3 \quad (112)$$

$$d = D_{b_1} - \bar{R}_l \hat{s}(\hat{x}_p, \hat{\Xi}_l) \quad (113)$$

$$\delta y = \text{sign}(\hat{y}_7 - \hat{\Xi}_l \hat{x}_7^3) I_l \bar{R}_l \sqrt{(\hat{x}_7 - \hat{x}_p)^2 + (\hat{y}_7 - \hat{y}_p)^2} \quad (114)$$

$$\psi_t = \Psi_s + \frac{I_l 180}{\pi} \tan^{-1}(3\hat{\Xi}_l \hat{x}_p^2) \quad 0 \leq \psi_t < 360^\circ \quad (115)$$

$$\frac{1}{\rho} = \frac{I_l 6 \hat{\Xi}_l \hat{x}_p}{\bar{R}_l (1 + 9\hat{\Xi}_l^2 \hat{x}_p^4)^{3/2}} \quad (116)$$

Circular segment on the approach circle  $B_2C_2$  (seg. 7) defined by  $D_{b_2} \geq d > D_{c_2}$

$$x_8 = (x_2 - R_{lx_2}) \cos \Delta \Psi_f + (y_2 - R_{ly_2}) \sin \Delta \Psi_f \quad (117)$$

$$y_8 = I_l [(x_2 - R_{lx_2}) \sin \Delta \Psi_f - (y_2 - R_{ly_2}) \cos \Delta \Psi_f] \quad (118)$$

$$\nu = \frac{180}{\pi} \tan^{-1} \left( \frac{-x_8}{y_8} \right) \quad 0 \leq \nu < 360^\circ \quad (119)$$

$$d = D_{c_2} + \frac{\pi}{180} \bar{R}_l (\nu - E_l) \quad (120)$$

$$l_l = \sqrt{x_8^2 + y_8^2} \quad (121)$$

$$\delta y = I_l (\bar{R}_l - l_l) \quad (122)$$

$$\psi_t = \Psi_f - I_l \nu \quad 0 \leq \psi_t < 360^\circ \quad (123)$$

$$\frac{1}{\rho} = \frac{I_l}{\bar{R}_l} \quad (124)$$

where  $(x_8, y_8)$  are the coordinates of the aircraft in coordinate frame 8 (fig. 2).

For segments  $C_2C_1$  and  $C_1S$ , the normalized coordinates of the aircraft  $(\hat{x}_9, \hat{y}_9)$ , in coordinate frame 9 (fig. 2), are given by

$$\hat{x}_9 = -[(x_2 - C_{x_2}) \cos \Delta \Psi_f + (y_2 - C_{y_2}) \sin \Delta \Psi_f] / \bar{R}_l + \hat{\Upsilon}_l \quad (125)$$

$$\hat{y}_9 = I_l [(y_2 - C_{y_2}) \cos \Delta \Psi_f - (x_2 - C_{x_2}) \sin \Delta \Psi_f] / \bar{R}_l \quad (126)$$

Turn-exit blending curve from the approach circle  $C_2C_1$  (seg. 8) defined by  $D_{c_2} \geq d > D_{c_1}$

$$\hat{x}_p = \hat{x}_9 \left[ 1 + \frac{3\hat{\Xi}_l \hat{x}_9 (\hat{y}_9 - \hat{\Xi}_l \hat{x}_9^3)}{1 - 3\hat{\Xi}_l \hat{x}_9 (2\hat{y}_9 - 5\hat{\Xi}_l \hat{x}_9^3)} \right] \quad (127)$$

$$\hat{y}_p = \hat{\Xi}_l \hat{x}_p^3 \quad (128)$$

$$d = D_{c_1} + \bar{R}_l \hat{s}(\hat{x}_p, \hat{\Xi}_l) \quad (129)$$

$$\delta y = \text{sign}(\hat{y}_9 - \hat{\Xi}_l \hat{x}_9^3) I_l \bar{R}_l \sqrt{(\hat{x}_9 - \hat{x}_p)^2 + (\hat{y}_9 - \hat{y}_p)^2} \quad (130)$$

$$\psi_t = \Psi_f - \frac{I_l 180}{\pi} \tan^{-1} (3\hat{\Xi}_l \hat{x}_p^2) \quad 0 \leq \psi_t < 360^\circ \quad (131)$$

$$\frac{1}{\rho} = \frac{I_l 6 \hat{\Xi}_l \hat{x}_p}{\bar{R}_l (1 + 9 \hat{\Xi}_l^2 \hat{x}_p^4)^{3/2}} \quad (132)$$

Final straight segment  $C_1S$  (seg. 9) defined by  $D_{c_1} \geq D$

$$d = D_{c_1} + \bar{R}_l \hat{x}_9 \quad (133)$$

$$\delta y = I_l \bar{R}_l \hat{y}_9 \quad (134)$$

$$\psi_t = \Psi_f \quad 0 \leq \psi_t < 360^\circ \quad (135)$$

$$\frac{1}{\rho} = 0 \quad (139)$$

The quantity  $\hat{s}(\hat{x}_p, \hat{\Xi})$  is the normalized distance of the point  $(\hat{x}_p, \hat{y}_p)$ , measured along the blending curve from the point where the transition curve and a straight segment meet, and is given by

$$\hat{s}(\hat{x}_p, \hat{\Xi}) = \hat{x}_p + 0.9\hat{\Xi}^2\hat{x}_p^5 - 1.125\hat{\Xi}^4\hat{x}_p^9 \quad (140)$$

## VERTICAL FLIGHTPATH SYNTHESIS

Vertical guidance, like lateral guidance, is provided by the ghost-aircraft symbol. At the instant of guidance select, the vertical flightpath is defined as shown in figure 4. This flightpath consists of a constant-altitude segment,  $AJ_1$ , at the altitude of flightpath select; an initial approach segment,  $J_2J_3$ , with a constant flightpath angle,  $\Gamma$ ; and a constant altitude segment,  $J_4S$ . These straight segments are connected by the circular arc segments  $J_1J_2$  and  $J_3J_4$ .

### Required Data

The following information must be provided to the system in order to define this flightpath:

$D_{J_\beta}$	distance from S to $J_\beta$
$H$	hover altitude
$R_{v_1}$	radius of segment $J_1J_2$
$R_{v_2}$	radius of segment $J_3J_4$
$\Gamma$	flightpath angle

These quantities are preset by the pilot, with suggested default values given by

$$D_{J_\beta} = 600 \text{ ft}$$

$$H = 50 \text{ ft}$$

$$R_{v_1} = 90000 \text{ ft}$$

$$R_{v_2} = 22500 \text{ ft}$$

$$\Gamma = -3 \text{ deg}$$

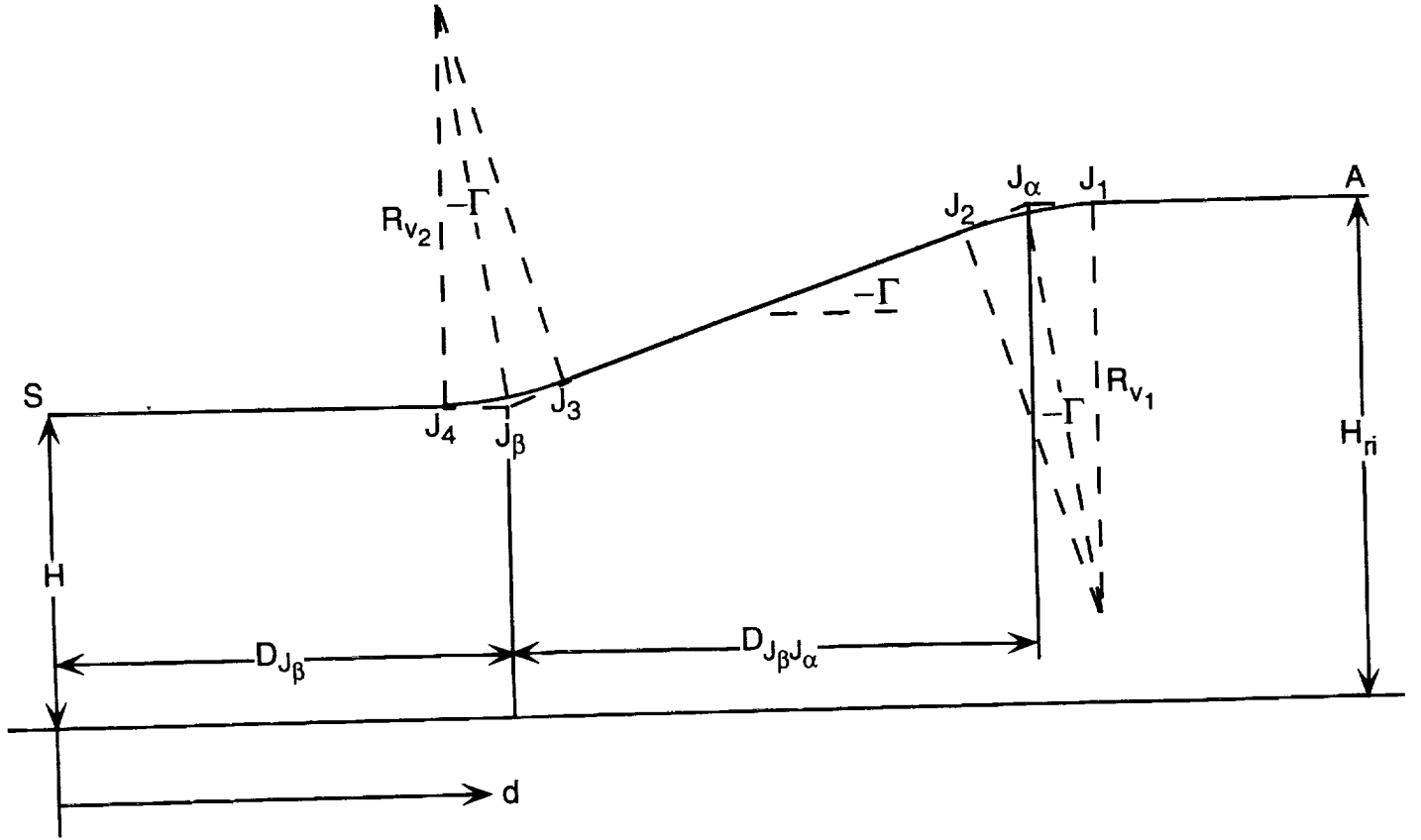


Figure 4. Vertical flightpath geometry.

### Calculations at Flightpath Select

From figure 4, the distance,  $D_{J_\beta J_\alpha}$ , from point  $J_\beta$  to point  $J_\alpha$  is given by

$$D_{J_\beta J_\alpha} = (H - H_{ri}) / \tan \Gamma \quad (141)$$

where  $H_{ri}$  is the aircraft's altitude at flightpath select. Also, from figure 4, the ranges at the points  $J_\beta$ ,  $J_\alpha$ ,  $J_4$ ,  $J_3$ ,  $J_1$ , and  $J_2$  are given by

$$D_{J_\alpha} = D_{J_\beta} + D_{J_\beta J_\alpha} \quad (142)$$

$$D_{J_4} = D_{J_\beta} + R_{v_2} \tan \Gamma / 2 \quad (143)$$

$$D_{J_3} = D_{J_4} - R_{v_2} \sin \Gamma \quad (144)$$

$$D_{J_1} = D_{J_\alpha} - R_{v_1} \tan \Gamma / 2 \quad (145)$$

$$D_{J_2} = D_{J_1} + R_{v_1} \sin \Gamma \quad (146)$$

and the corresponding altitudes are given by

$$H_{J_\beta} = H \quad (147)$$

$$H_{J_\alpha} = H_{ri} \quad (148)$$

$$H_{J_4} = H \quad (149)$$

$$H_{J_3} = H + R_{v_2}(1 - \cos \Gamma) \quad (150)$$

$$H_{J_1} = H_{ri} \quad (151)$$

$$H_{J_2} = H_{ri} - R_{v_1}(1 - \cos \Gamma) \quad (152)$$

### Vertical Guidance

The elevation angle of the ghost aircraft relative to the real aircraft,  $\eta_g$ , is expressed in reference 1 (eq. 19) as

$$\eta_g = \frac{180}{\pi} \tan^{-1} \left( \frac{h_g - h}{\delta x_{gh}} \right) \quad (153)$$

where

$h_g$	altitude of the ghost aircraft
$h$	altitude of the aircraft
$\delta x_{gh}$	lead distance of the ghost for vertical tracking

The ghost altitude is given by

$$h_g = h_r + \delta x_{gh} k_{wg} \tan \gamma_t \quad (154)$$

where

$h_r$	aircraft reference altitude
$\gamma_t$	reference flightpath angle at the aircraft's range
$k_{wg}$	ghost lead blending gain

From equations 153 and 154,  $\eta_g$  may be expressed as

$$\eta_g = \tan^{-1} \left( k_{wg} \tan \gamma_t - \frac{\delta h}{\delta x_{gh}} \right) \quad (155)$$

where  $\delta h = h - h_r$  is the altitude error of the aircraft relative to the reference flightpath.

Determination of  $\eta_g$ , therefore, requires knowledge of the altitude error,  $\delta h$ , and the reference flightpath angle,  $\gamma_t$ . These quantities depend on which segment of the reference flightpath the aircraft is located in.

Within segment AJ<sub>1</sub>, defined by  $D_a \geq d > D_{J_1}$

$$\gamma_t = 0 \quad (156)$$

$$\delta h = h - H_{ri} \quad (157)$$

Within segment J<sub>1</sub>J<sub>2</sub>, defined by  $D_{J_1} \geq d > D_{J_2}$

$$\gamma_t = \tan^{-1}[d - D_{J_1})/R_{v_1}] \quad (158)$$

$$\delta h = h - H_{ri} + R_{v_1}(1 - \cos \gamma_t) \quad (159)$$

Within segment J<sub>2</sub>J<sub>3</sub>, defined by  $D_{J_2} \geq d > D_{J_3}$

$$\gamma_t = \Gamma \quad (160)$$

$$\delta h = h - H_{J_3} + (d - D_{J_3}) \tan \gamma_t \quad (161)$$

Within segment J<sub>3</sub>J<sub>4</sub>, defined by  $D_{J_3} \geq d > D_{J_4}$

$$\gamma_t = \Gamma - \tan^{-1}(d - D_{J_3})/R_{v_2}) \quad (162)$$

$$\delta h = h - H_{J_4} - R_{v_2}(1 - \cos \gamma_t) \quad (163)$$

Within segment J<sub>4</sub>S, defined by  $D_{J_4} \geq d > 0$

$$\gamma_t = 0 \quad (164)$$

$$\delta h = h - H \quad (165)$$

## HUD LATERAL SCALING AND LIMITING

### HUD Lateral Scaling

The problem of HUD lateral scaling was discussed in reference 2, where it was pointed out that the method of scaling used in reference 1 resulted in an indication of large sideslip angles in steady, coordinated turns. This anomaly appears when the scaling factor,  $K_e$ , is applied to both the ghost and flightpath symbols in the Earth-fixed coordinate reference frame. On the other hand, it was shown, in reference 2, that although the sideslip anomaly can be avoided if the scaling factor is applied in the HUD reference frame, this introduces an even more undesirable anomaly. This latter problem manifests itself to the pilot as an anomalous vertical movement of the ghost symbol induced by aircraft roll. The instinctive reaction of the pilot to this vertical motion is to apply vertical control to counter it, only to find that when the aircraft is rolled back to level, the ghost symbol again moves vertically

in the reverse direction and the pilot must cancel the original vertical control input. At the time of preparation of reference 2 the dilemma of HUD lateral scaling had not been satisfactorily resolved.

It is clear, as stated in reference 2, that any type of lateral scaling will produce anomalies of one form or another. The major issue revolves around the question of which anomaly is the least objectionable. Considerations along this direction have led to the following, hopefully more rational, approach to the problem.

A key observation concerning this problem is that the only component of the ghost symbol lateral position that needs to be scaled is that due to the difference between the heading of the tangent to the reference flightpath,  $\psi_t$ , and the aircraft heading,  $\psi$ , since this is the component that results in the large ghost symbol displacement from the center of the HUD field of view. The component due to lateral tracking error,  $\delta y$ , is sufficiently small that it need not be scaled. This observation is not new and is, in fact, implied in reference 1, equation 23. However, a better way to implement it is required.

If there were no lateral error, then the elevation,  $\eta_g$ , and the unscaled azimuth,  $\mu_{g1}$ , are given by (ref. 1, eqs. 19 and 23)

$$\eta_g = \frac{180}{\pi} \tan^{-1} \left( \frac{h_g - h}{\delta x_{gh}} \right) \quad (166)$$

$$\mu_{g1} = (\psi_t - \psi) k_{wg} \quad (167)$$

After transformation to the HUD coordinate frame, the unlimited coordinates of the ghost ( $x_{g1}$ ,  $y_{g1}$ ) on the HUD are given by

$$x_{g1} = \mu_{g1} \cos \phi - (\eta_g - \theta) \sin \phi \quad (168)$$

$$y_{g1} = \mu_{g1} \sin \phi + (\eta_g - \theta) \cos \phi \quad (169)$$

where  $\theta$  and  $\phi$  are the aircraft pitch and roll, respectively.

With a lateral tracking error,  $\delta y$ , the ghost azimuth,  $\mu_g$ , is given by

$$\mu_g = (\psi_t - \psi) k_{wg} - \frac{180}{\pi} \tan^{-1} \left( \frac{\delta y}{\delta x_{gy}} \right) \quad (170)$$

and, again, after transformation to the HUD coordinate frame, the unlimited coordinates of the ghost ( $x_g$ ,  $y_g$ ) on the HUD are

$$x_g = \mu_g \cos \phi - (\eta_g - \theta) \sin \phi \quad (171)$$

$$y_g = \mu_g \sin \phi + (\eta_g - \theta) \cos \phi \quad (172)$$

The effect of the lateral tracking error on the HUD is represented by the quantity  $x_g - x_{g1}$ .

Since only the lateral position of the ghost with no lateral tracking error needs to be scaled, a suitable scaling can be accomplished by locating the ghost on the HUD laterally using the relationship

$$x_g^s = K_\epsilon x_{g1} + (x_g - x_{g1}) \quad (173)$$

However, it is not sufficient to merely scale the ghost symbol position on the HUD laterally, since moving the ghost symbol in this way also changes its position relative to the horizon. The situation is shown in figure 5, from which it is clear that the vertical position of the ghost symbol on the HUD,  $y_g^s$ , must be reduced from its unscaled value,  $y_g$ , according to the equation

$$y_g^s = y_g - (x_g - x_g^s) \tan \phi \quad (174)$$

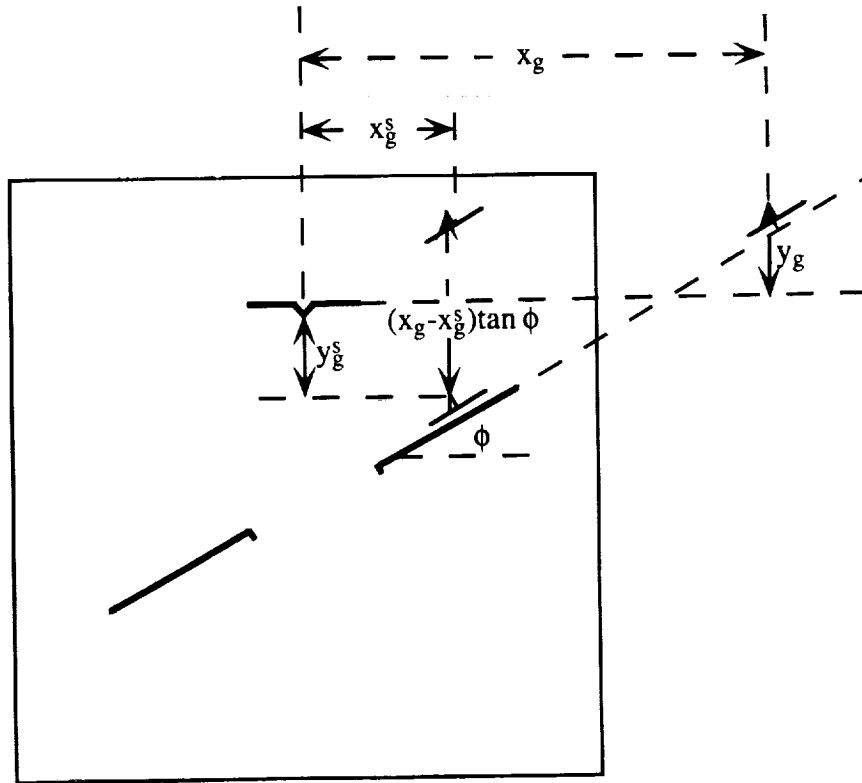


Figure 5. Lateral scaling of the ghost-aircraft symbol.



The aim of equations 173 and 174 is to scale the ghost position laterally while ensuring that the relationship of the ghost aircraft to the horizon, as represented by the elevation of the scaled ghost symbol,  $\eta_g^s$ , remains unchanged from its unscaled value,  $\eta_g$ . That this is the case may be shown explicitly by transforming the ghost symbol positions,  $x_g^s$  and  $y_g^s$ , back to the Earth-fixed coordinate frame, as follows:

$$\eta_g^s - \theta = y_g^s \cos \phi - x_g^s \sin \phi \quad (175)$$

Substituting for  $x_g^s$  and  $y_g^s$  from equations 173 and 174 gives

$$\eta_g^s - \theta = [y_g - (x_g - x_g^s) \tan \phi] \cos \phi - x_g^s \sin \phi \quad (176)$$

which reduces to

$$\eta_g^s - \theta = y_g \cos \phi - x_g \sin \phi = \eta_g - \theta \quad (177)$$

from which it follows that  $\eta_g^s = \eta_g$ , as required.

To make the flightpath and ghost symbols compatible, the flightpath symbol must be scaled and transformed in the same way as the ghost; thus

$$x_f^s = K_\epsilon x_f \quad (178)$$

$$y_f^s = y_f - (x_f - x_f^s) \tan \phi \quad (179)$$

where  $x_f$  and  $y_f$  are the unscaled positions of the flightpath symbols on the HUD and  $x_f^s$  and  $y_f^s$  are the corresponding scaled values. But, from the HUD geometry, the unscaled ghost coordinates,  $x_f$  and  $y_f$ , are equal to the inertial angles of sideslip,  $\beta_i$ , and angle of attack,  $\alpha_i$ , respectively. Therefore, by equation 178, the indicated inertial sideslip angle,  $x_f^s$ , is less than its true value by the scale factor  $K_\epsilon$  and, by equation 179, the indicated inertial angle of attack differs from its true value by the quantity  $(x_f - x_f^s) \tan \phi$  which, by equation 179 and the correspondence between  $x_f$  and  $\beta_i$ , is equal to  $\beta_i(1 - K_\epsilon) \tan \phi$ . It follows that if  $K_\epsilon = 0.3$ , the HUD flightpath symbol cannot provide an accurate measure of sideslip, but this may be preferable to indicating a large sideslip where none exists, as with the scaling of reference 1. It would appear that the lateral acceleration ball, located on top of the flightpath symbol (ref. 1), should be used to indicate sideslip. It also follows that the angle-of-attack indication is accurate only when either sideslip or the angle of bank is zero. If, for example, the sideslip angle is 10 deg and the bank angle is 30 deg then the error in angle of attack is 4 deg. It is the errors in sideslip angle and angle of attack that are the anomalies with this approach to the HUD lateral scaling. However, these anomalies may be less objectionable than those resulting from the alternative scaling methods discussed in references 1 and 2.

## HUD Limiting

Implementation of the previously described HUD scaling method has shown an error in the way that lateral HUD limiting was performed in reference 1. This error was particularly evident in the behavior of the ghost symbol. When the ghost was limited and the aircraft was oscillated in roll, the symbol was observed to move vertically in synchronization with the roll. The reason for this behavior is illustrated in figure 6. The limiting process specified in reference 1 involved projecting the ghost from its unlimited lateral position along a line parallel to the horizontal axis of the HUD. It is evident from figure 6 that if the elevation of the ghost is fixed, then, as the horizon line rotates on the HUD in response to roll commands, the ghost symbol will traverse along the lateral edge of the display, giving the impression that the elevation of the ghost is changing. The proposed approach to the lateral limiting, when the ghost is in the zones to the right of line FBCG or to the left of line EADH (fig. 6), is to assume that it will be acquired by using roll control and, therefore, that the best indication of its position is to project it along a line parallel to the horizon line, from its unlimited position, to the closest lateral edge of the display. This projection is accomplished with the following pseudocode:

$$\text{IF } x_g^s > X_{max} \quad x_g^s \Leftarrow X_{max} \quad (180)$$

$$\text{IF } x_g^s < X_{min} \quad x_g^s \Leftarrow X_{min} \quad (181)$$

$$y_g^s = y_g - (x_g - x_g^s) \tan \phi \quad (182)$$

where  $X_{max}$  and  $X_{min}$  are the maximum and minimum values of  $x_g^s$ .

Limiting when the ghost is in the vertical zones EABF or HDCG (fig. 6) is performed assuming that the ghost will be acquired using vertical control. This limiting is given by the following pseudocode:

$$\text{IF } y_g^s > Y_{max} \quad y_g^s \Leftarrow Y_{max} \quad (183)$$

$$\text{IF } y_g^s < Y_{min} \quad y_g^s \Leftarrow Y_{min} \quad (184)$$

where  $Y_{max}$  and  $Y_{min}$  are the maximum and minimum values of  $y_g^s$ .

Although the flightpath symbol only very rarely passes outside the field of view of the HUD, it is appropriate to use the same limiting process as for the ghost symbol.

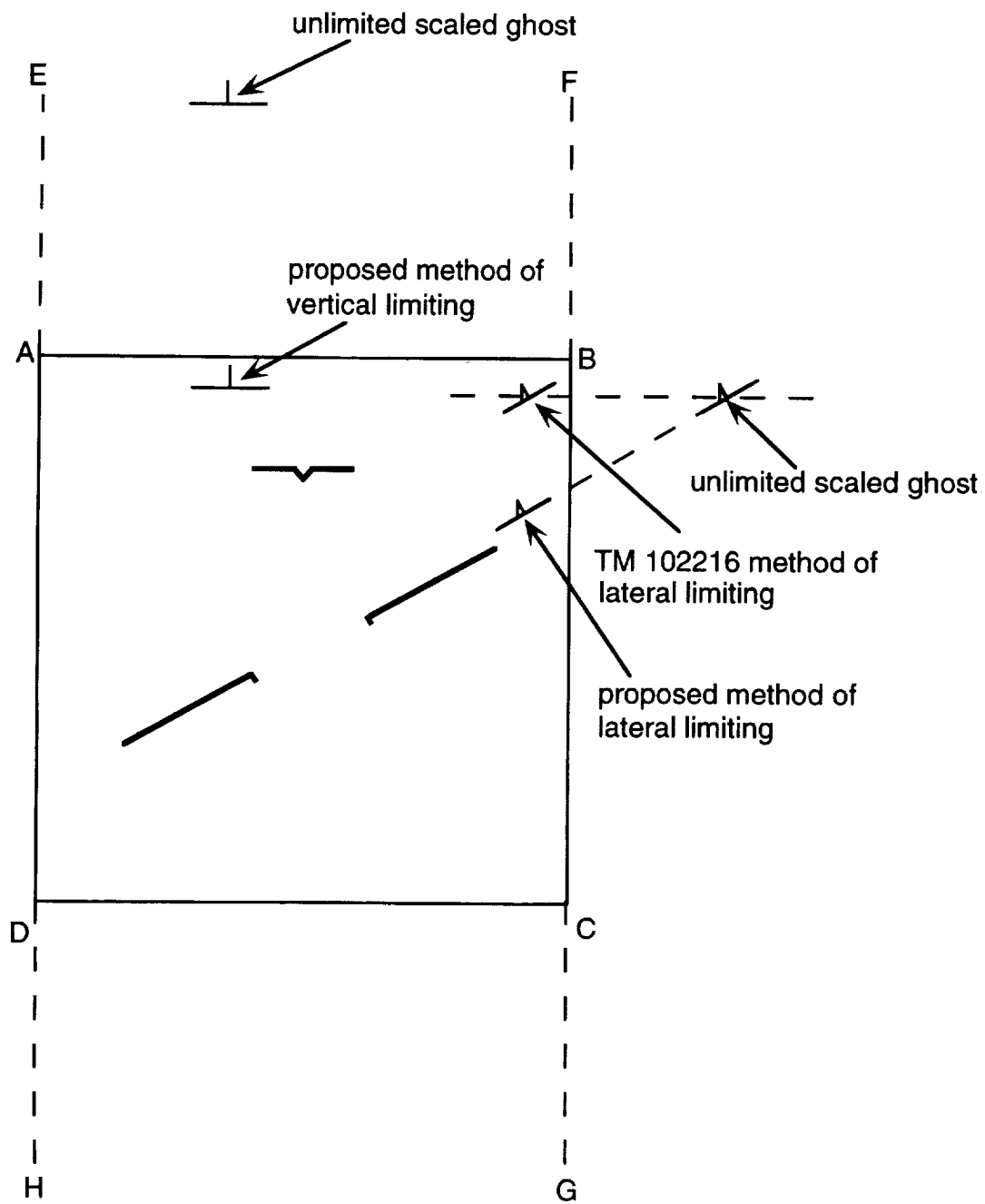


Figure 6. Limiting of the ghost-aircraft symbol.

## REFERENCES

1. Merrick, Vernon K.; Farris, Glenn G.; and Vanags, Andrejs A.: A Head Up Display for Application to V/STOL Aircraft Approach and Landing. NASA TM-102216, Jan. 1990.
2. Merrick, Vernon K.: Some VTOL Pilot Display Drive-Law Problems and Solutions. NASA TM-104027, Oct. 1993.
3. Dorr, D. W.; Morales III, E.; and Merrick, V. K.: Simulation and Flight Test Evaluation of Head-Up-Display Guidance for Harrier Approach Transitions. AIAA Paper 92-4233, Aug. 1992.

## APPENDIX

### COMPUTER-GRAPHIC FLIGHTPATH

A graphical representation of the nominal horizontal flightpath defined by equations 1-46 is provided. The associated computer program has been written for an Apple Macintosh (68XXX; System 7.0 or higher) and resides on a standard 3.5 inch floppy disk provided with the report. The program runs in 1250 kilobytes of memory, but requires only 52 kilobytes of disk space.

#### Operating Instructions

A double click on the flightpath icon loads the program and produces a screen similar to figure 7. This figure shows a clockwise horizontal flightpath relative to an upward pointing north, for a default set of input parameters. Also shown is a column of six icons which provide additional information. The first of these, read in downward order, provides a report giving the values of the input parameters and a set of output parameters describing the resultant flightpath, for both clockwise and counterclockwise approach circles (fig. 8). The parameters are given below along with the corresponding algebraic symbols.

#### Inputs

Parameters	Symbols	Definition
X1_FS		$x$ coordinate of the aircraft at flightpath select in coordinate frame 1 (point $A_0$ in fig. 1), ft
Y1_FS		$y$ coordinate of the aircraft at flightpath select in coordinate frame 1 (point $A_0$ in fig. 1), ft
SX1	$S_{x_1}$	$x$ coordinate of the station-keeping point in coordinate frame 1, ft
SY1	$S_{y_1}$	$y$ coordinate of the station-keeping point in coordinate frame 1, ft
DI	$D_i$	nominal length of the initial flightpath segment (seg. 1), ft
DC	$D_c$	nominal length of the final straight segment, ft
RLMIN	$R_{l(min)}$	minimum nominal radius of the flightpath approach circle, ft
RAMIN	$R_{a(min)}$	minimum nominal radius of the flightpath acquiring circle, ft
RMAX	$R_{(max)}$	maximum nominal radius of either the acquiring or the approach circle, ft
DELTAD	$\Delta D$	minimum desirable distance along the approach circle, ft
PSIFD	$\Psi_f$	heading of the final flightpath segment, deg
PSILPD	$\Psi$	landing pad heading, deg
PSIVD	$\Psi_v$	heading of the aircraft's velocity vector, deg

## Outputs

Parameters	Symbols	Definition
NULD	$N_l$	nominal angle subtended at the center of the approach circle by the segment of the flightpath lying on the approach circle, deg
NUAD	$N_a$	nominal angle subtended at the center of the acquiring circle by the segment of the flightpath lying on the acquiring circle, deg
A0X1		$x$ coordinate of point $A_0$ (fig. 1) in coordinate frame 1, ft
A0Y1		$y$ coordinate of point $A_0$ (fig. 1) in coordinate frame 1, ft
AX1		$x$ coordinate of point A (fig. 1) in coordinate frame 1, ft
AY1		$y$ coordinate of point A (fig. 1) in coordinate frame 1, ft
DX1		$x$ coordinate of point D (fig. 1) in coordinate frame 1, ft
DY1		$y$ coordinate of point D (fig. 1) in coordinate frame 1, ft
BX1		$x$ coordinate of point B (fig. 1) in coordinate frame 1, ft
BY1		$y$ coordinate of point B (fig. 1) in coordinate frame 1, ft
CX1		$x$ coordinate of point C (fig. 1) in coordinate frame 1, ft
CY1		$y$ coordinate of point C (fig. 1) in coordinate frame 1, ft
SX2		$x$ coordinate of point S (fig. 1) in coordinate frame 2, ft
SY2		$y$ coordinate of point S (fig. 1) in coordinate frame 2, ft
RAX1		$x$ coordinate of the center of the acquiring circle in frame 1, ft
RAY1		$y$ coordinate of the center of the acquiring circle in frame 1, ft
RLX1		$x$ coordinate of the center of the approach circle in frame 1, ft
RLY1		$y$ coordinate of the center of the approach circle in frame 1, ft
RADLOCA	$R_a$	nominal radius of the acquiring circle, ft
RADLOCL	$R_l$	nominal radius of the approach circle, ft
LENGTHDB	$l_{db}$	nominal length of the straight segment tangential to both the acquiring and approach circles, ft
CLOCKA	$I_a$	indicates clockwise ( $I_a = +1$ ) or counterclockwise ( $I_a = -1$ ) acquiring circle
CLOCKL	$I_l$	indicates clockwise ( $I_l = +1$ ) or counterclockwise ( $I_l = -1$ ) approach circle
AMGLEMD	$\alpha_m$	angle between a line connecting the centers of the acquiring and approach circles and the common tangent to the two circles, deg
DELPSIALD	$\delta\psi_{al}$	angle between the line connecting the centers of the acquiring and approach circles and the $x$ axis of frame 2, deg

To view either the clockwise or counterclockwise approach circle flightpaths, it is required to click on either the second or third icon, respectively. For the default parameters, the result of clicking on the counterclockwise (third) icon is shown in figure 9. A click on the fifth icon will present the clockwise and counterclockwise approach circle flightpaths

simultaneously (fig. 10). The shorter of the two paths can be viewed by clicking on the fourth icon.

The input parameters can be modified in two ways. A click on either the final or initial straight segments will produce an effect similar to that shown in figure 11, where the click has been made on the final straight segment. The segment selected becomes a dashed line and three markers appear, one at each end of the line and one at its midpoint. A click and drag on one or another of these markers permits the segment to be stretched, rotated, or translated, as indicated in figure 11. When a change is in progress the parameter being varied, along with its current value, is shown in the upper left hand corner of the picture. A click on the landing pad produces a similar effect, except that the stretching feature is not provided, since it is not needed. The scale of the flightpath can be changed, if required, by clicking on the scale rule. Markers appear at each end of the scale and a click and drag on the right hand one changes the scale. The other marker is used to move the scale to a more convenient location. The alternate way to change the input parameters is to click on the "set input" from the "options" menu. This action produces the table of inputs shown in figure 12. The parameter values shown in the table can be modified with the mouse.

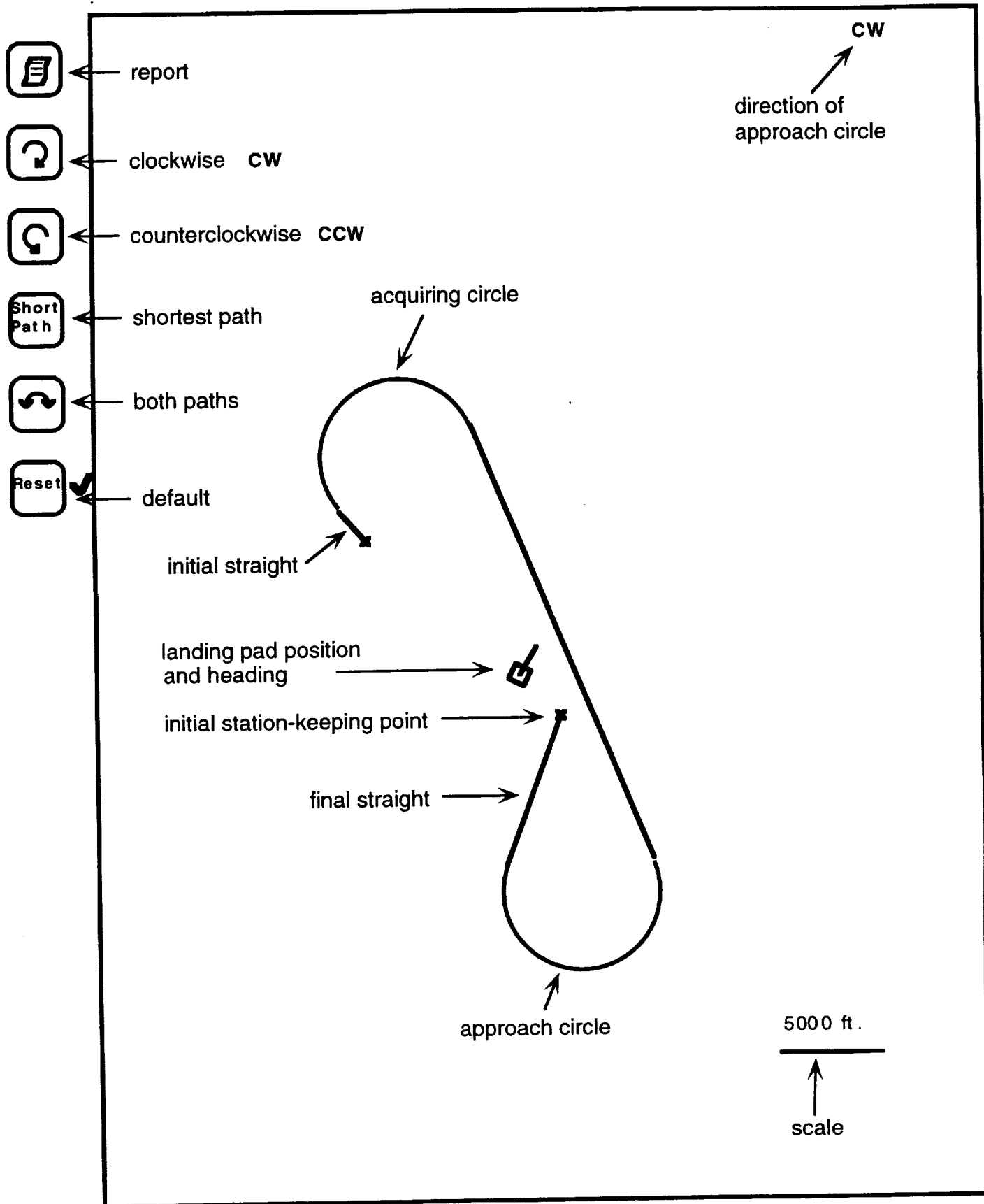


Figure 7. Screen after startup or after selection of reset.





### Inputs

X1\_FS = 6750 Y1\_FS = -7600  
SX1 = -2000 SY1 = 2000  
DI = 2000 DC = 8000  
RLMIN = 4000  
RAMIN = 4000  
RMAX = 30000  
DELTAD = 2000  
PSIFD = 2.0  
PSILPD = 3.0  
PSIVD = 3.20

### Outputs

#### CW:

NULD = 2.22 NUAD = 1.98  
A0X1 = 6750 A0Y1 = -7600  
AX1 = 8.282 AY1 = -8886  
DX1 = 1.2361 DY1 = -2116  
BX1 = -9378 BY1 = 6.728  
CX1 = -9518 CY1 = -736  
SX2 = -732 SY2 = 2.732  
RAX1 = 10853 RAY1 = -5821  
RLX1 = -10886 RLY1 = 3023  
RADLOCA = 4000 RADLOCL = 4000  
LENGTHDB = 23469  
CLOCKA = 1 CLOCKL = 1  
ANGLEMD = 0.0000 DELPSIALD = 127.8623

#### CCW:

NULD = 1.32 NUAD = 1.68  
A0X1 = 6750 A0Y1 = -7600  
AX1 = 8.282 AY1 = -8886  
DX1 = 3.816 DY1 = -15472  
BX1 = -10044 BY1 = -8018  
CX1 = -9518 CY1 = -736  
SX2 = -732 SY2 = 2.732  
RAX1 = 5711 RAY1 = -11950  
RLX1 = -8149 RLY1 = -4495  
RADLOCA = 4000 RADLOCL = 4000  
LENGTHDB = 15738  
CLOCKA = -1 CLOCKL = -1  
ANGLEMD = 0.0000 DELPSIALD = 121.7266

note: see text for definition  
of symbols

Figure 8. Report giving numerical values for flightpath parameters.

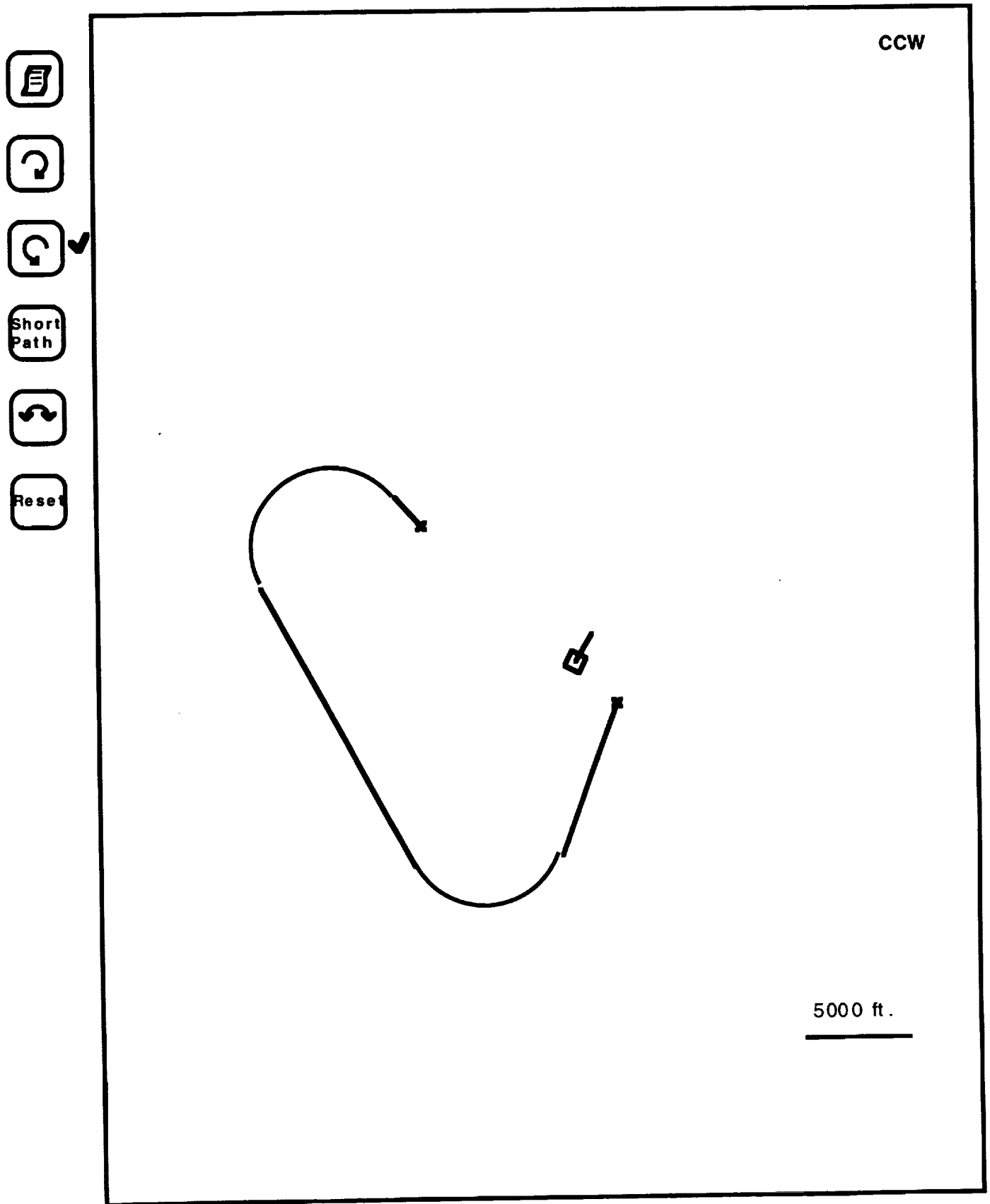


Figure 9. Selection of counterclockwise option with reset parameters.

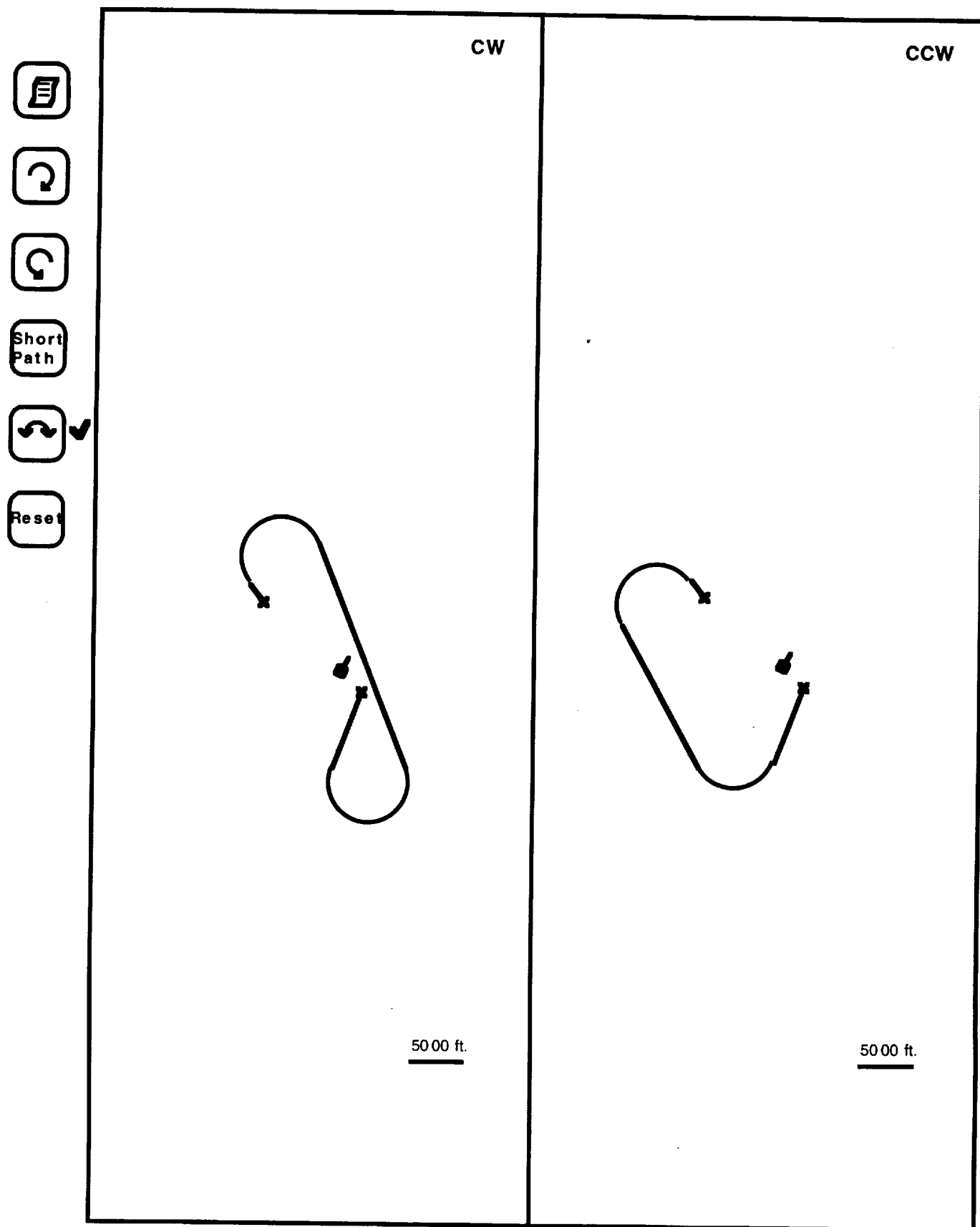
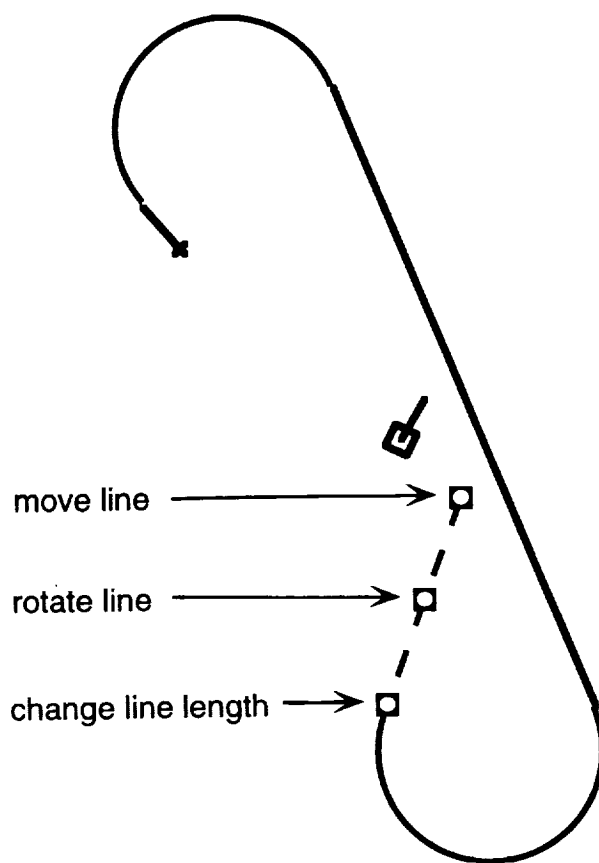


Figure 10. Selection of both clockwise and counterclockwise options with reset parameters.



CW



5000 ft.



Figure 11. Modification of the final approach segment using a mouse.

H1_FS	6750	Y1_FS	-7600
SK1	-2000	SY1	2000
DI	2000	DC	8000
RLMIN	4000	RAMIN	4000
RMAX	30000	PSIFD	20
DELTAD	2000	PSIUD	320
PSILPD	30		
Cancel		OK	

Figure 12. Input parameter table after selection of "set input" from the "options" menu.

**REPORT DOCUMENTATION PAGE**Form Approved  
OMB No. 0704-0188

Public reporting burden for this collection of information is estimated to average 1 hour per response, including the time for reviewing instructions, searching existing data sources, gathering and maintaining the data needed, and completing and reviewing the collection of information. Send comments regarding this burden estimate or any other aspect of this collection of information, including suggestions for reducing this burden, to Washington Headquarters Services, Directorate for Information Operations and Reports, 1215 Jefferson Davis Highway, Suite 1204, Arlington, VA 22202-4302, and to the Office of Management and Budget, Paperwork Reduction Project (0704-0188), Washington, DC 20503.

<b>1. AGENCY USE ONLY (Leave blank)</b>		<b>2. REPORT DATE</b> April 1995	<b>3. REPORT TYPE AND DATES COVERED</b> Technical Memorandum	
<b>4. TITLE AND SUBTITLE</b> Flightpath Synthesis and HUD Scaling for V/STOL Terminal Area Operations			<b>5. FUNDING NUMBERS</b>  505-59-36	
<b>6. AUTHOR(S)</b> Vernon K. Merrick and James A. Jeske				
<b>7. PERFORMING ORGANIZATION NAME(S) AND ADDRESS(ES)</b> Ames Research Center Moffett Field, CA 94035-1000			<b>8. PERFORMING ORGANIZATION REPORT NUMBER</b>  A-950052	
<b>9. SPONSORING/MONITORING AGENCY NAME(S) AND ADDRESS(ES)</b> National Aeronautics and Space Administration Washington, DC 20546-0001			<b>10. SPONSORING/MONITORING AGENCY REPORT NUMBER</b>  NASA TM-110348	
<b>11. SUPPLEMENTARY NOTES</b> Point of Contact: James A. Jeske, Ames Research Center, MS 211-2, Moffett Field, CA 94035-1000 (415) 604-5934				
<b>12a. DISTRIBUTION/AVAILABILITY STATEMENT</b>  Unclassified — Unlimited Subject Category 04			<b>12b. DISTRIBUTION CODE</b>	
<b>13. ABSTRACT (Maximum 200 words)</b> <p>A two circle horizontal flightpath synthesis algorithm for Vertical/Short Takeoff and Landing (V/STOL) terminal area operations is presented. This algorithm provides a flightpath that is tangential to the aircraft's velocity vector at the instant of flightpath select and has continuous curvature. The algorithm corrects deficiencies noted in tests conducted with the V/STOL Systems Research Aircraft (VSRA) using a single circle algorithm described in NASA TM 104027. In addition, a more general vertical flightpath synthesis algorithm is presented, aimed primarily at minimizing the rapid increase of pilot workload during the final phase of decelerating transition just prior to acquiring the station-keeping point. Finally, a new technique for lateral scaling of a V/STOL Head Up Display (HUD) is presented, aimed at minimizing the inevitable anomalies that such scaling produces.</p> <p>All the above named items have been tested in flight with the VSRA, and all have produced improvements.</p>				
<b>14. SUBJECT TERMS</b> VTOL, Head up display, HUD, Landing			<b>15. NUMBER OF PAGES</b> 46	
			<b>16. PRICE CODE</b> A03	
<b>17. SECURITY CLASSIFICATION OF REPORT</b> Unclassified	<b>18. SECURITY CLASSIFICATION OF THIS PAGE</b> Unclassified	<b>19. SECURITY CLASSIFICATION OF ABSTRACT</b>	<b>20. LIMITATION OF ABSTRACT</b>	